

---

# HIGHER-ORDER HIT-&-RUN SAMPLERS FOR LINEARLY CONSTRAINED DENSITIES

---

Richard D. Paul<sup>1,2</sup> Anton Stratmann<sup>1</sup> Johann F. Jadebeck<sup>1</sup> Martin Beyß<sup>1</sup>

Hanno Scharr<sup>1</sup> David Rügamer<sup>2,3</sup> Katharina Nöh<sup>1</sup>

<sup>1</sup> Forschungszentrum Jülich

<sup>2</sup> Department of Statistics, LMU Munich

<sup>3</sup> Munich Center for Machine Learning (MCML)

## ABSTRACT

Markov chain Monte Carlo (MCMC) sampling of densities restricted to linearly constrained domains is an important task arising in Bayesian treatment of inverse problems in the natural sciences. While efficient algorithms for uniform polytope sampling exist, much less work has dealt with more complex constrained densities. In particular, gradient information as used in unconstrained MCMC is not necessarily helpful in the constrained case, where the gradient may push the proposal's density out of the polytope. In this work, we propose novel constrained sampling algorithms, which combine strengths of higher-order information, like the target log-density's gradients and curvature, with the Hit-&-Run proposal, a simple mechanism which guarantees the generation of feasible proposals, fulfilling the linear constraints. Our extensive experiments demonstrate improved sampling efficiency on complex constrained densities over various constrained and unconstrained samplers.

## 1 Introduction

*Hit-&-Run* (HR, Smith, 1984; Bélisle et al., 1993) is a well-established *Markov chain Monte Carlo* (MCMC) method for sampling from probability densities defined on constrained domains. HR is applied in diverse domains like operations research (Tervonen et al., 2013), cosmology (Lubini et al., 2013), systems biology (Herrmann et al., 2019; Theorell et al., 2017) and ecology (Gellner et al., 2023), where modelling principles give rise to linearly constrained domains. Moreover, HR has been used as a building block in advanced sampling algorithms (Theorell and Nöh, 2019; Ashton et al., 2022; Łatuszyński and Rudolf, 2024). Its main strength for constrained sampling is the algorithm's guarantee to only generate feasible samples. Lovász and Vempala (2006) prove HR mixes rapidly for uniform sampling of bounded and convex linearly constrained domains, referred to as convex polytopes.

However, real-world inverse problems, e.g. those arising from Bayesian inference (Theorell et al., 2017; Bohra-Slater et al., 2023), lead to more complex non-uniform densities. These densities present additional sampling challenges such as strong nonlinear correlations between

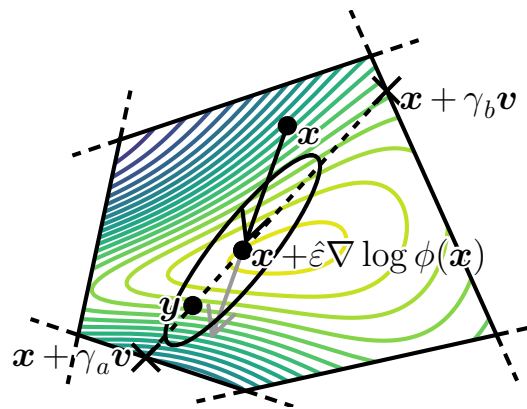


Figure 1: Our proposed smLHR sampler preconditions the direction using local curvature and clips the natural gradient step to prevent it from leaving the feasible region.

variables, or concentration of measure in small regions of the constrained domain. For sampling densities defined on unconstrained domains, the incorporation of higher-order information of the density has shown great success in dealing with these challenges. Prominent examples are gradient-guided samplers such as the *Metropolis-adjusted Langevin algorithm* (MALA, Rossky et al., 1978) and *Hamiltonian Monte Carlo* (HMC, Duane et al., 1987), or curvature-based preconditioning as in *Riemannian Manifold MALA* (mMALA) and *Riemannian HMC* (RHMC, Girolami and Calderhead, 2011). In addition, recent advances in automatic differentiation have greatly benefited the calculation of the higher-order information (Baydin et al., 2018).

To leverage higher-order information for sampling densities defined on convexly constrained domains, alternatives to HR have been proposed. (Kook et al., 2022) introduce a constrained version of Riemannian HMC for sampling log-concave densities, but test it only for uniform problems. Recently, (Srinivasan et al., 2024) proposed the first-order *Metropolis-adjusted Preconditioned Langevin algorithm* (MAPLA). Built upon Girolami and Calderhead (2011), MAPLA preconditions a Gaussian proposal density with a metric induced by the log-barrier function (Fiacco and McCormick, 1990) to incorporate information about the constraints instead of the curvature information of the domain-constrained density. Although MAPLA aims to guide the sampling such that proposed samples respect the constraints, its proposal density remains Gaussian, thus admitting some positive probability of proposing infeasible samples. This raises the question whether higher-order algorithms that only propose feasible samples improve the sampling efficiency for non-uniform constrained sampling problems.

**Contribution** In this work, we propose feasible higher-order samplers, which have positive proposal density just exactly on the convex-constrained domain. To this end, we combine the HR proposal mechanism with existing first- and second-order samplers like MALA and the simplified mMALA (Girolami and Calderhead, 2011). As a result, we develop three new samplers *Langevin Hit-&-Run* (LHR), *simplified manifold Hit-&-Run* (smHR), and *simplified manifold Langevin Hit-&-Run* (smLHR). Our approach is mainly driven by the observation that a Gaussian random variable can be sampled in a HR-like fashion by decomposing it into direction and magnitude. We provide theoretical analysis to prove convergence of our samplers to the desired target densities. We numerically evaluate our algorithms on a systematically constructed benchmark consisting of 2240 problems, which combine parametrizable polytopes and probability densities of varying geometry or ill condition, as well as on real-world examples from the field of Bayesian  $^{13}\text{C}$  metabolic flux analysis ( $^{13}\text{C}$ -MFA, Theorell et al., 2017). Our results show that our combination of both the incorporation of higher-order information and the constraining of the proposal density by the HR proposal mechanism improve sampling efficiency.

## 2 Preliminaries

We consider the problem of MCMC sampling from smooth probability densities  $\pi(\mathbf{x})$  with support restricted to non-empty, convex-constrained domains

$$\mathcal{P} = \{\mathbf{x} \in \mathbb{R}^d : \mathbf{A}\mathbf{x} \leq \mathbf{b}\}, \quad (1)$$

defined by  $m$  linear constraints  $\mathbf{A}\mathbf{x} \leq \mathbf{b}$ , i.e.  $\mathbf{A} \in \mathbb{R}^{m \times d}$ ,  $\mathbf{b} \in \mathbb{R}^m$ . If  $\mathcal{P}$  is bounded, we refer to it as a *polytope*.

### 2.1 Metropolis-Hastings Algorithm

The *Metropolis-Hastings* (MH, Metropolis et al., 1953; Hastings, 1970) algorithm is a widely applied method to draw samples from a target density  $\pi : \mathbb{R}^d \rightarrow \mathbb{R}$ , even if access is only provided to some unnormalized density  $\varphi(\mathbf{x}) = Z\pi(\mathbf{x})$ , where  $Z$  is the normalization constant. It works by iteratively drawing samples, called *proposals*, from some proposal distribution  $\mathbf{y} \sim q(\cdot | \mathbf{x})$  conditional on  $\mathbf{x}$ , before “correcting” them to match the desired target distribution. To this end, the MH algorithm adds a filter that accepts or rejects transitions from  $\mathbf{x}$  to  $\mathbf{y}$  with acceptance probability

$$\alpha(\mathbf{y} | \mathbf{x}) = \min \left\{ 1, \frac{\varphi(\mathbf{y})}{\varphi(\mathbf{x})} \cdot \frac{Z}{Z'} \cdot \frac{q(\mathbf{x} | \mathbf{y})}{q(\mathbf{y} | \mathbf{x})} \right\}. \quad (2)$$

A sufficient condition for the convergence of this Markov chain is that  $q(\mathbf{y} | \mathbf{x}) > 0$  for any two states  $\mathbf{x}, \mathbf{y} \in \text{supp}(\pi)$  (Roberts and Rosenthal, 2004).

The MH algorithm is also applicable to constrained target densities  $\pi : \mathcal{P} \rightarrow \mathbb{R}$ , if we define an extension thereof with zero density for any state outside  $\mathcal{P}$ , i.e.  $\hat{\pi}(\mathbf{x}) := \mathbb{1}_{\mathcal{P}}(\mathbf{x})\pi(\mathbf{x})$ , where  $\mathbb{1}_{\mathcal{P}}$  is the indicator function on  $\mathcal{P}$ . Assuming that we start within  $\text{supp}(\pi) \subseteq \mathcal{P}$ , the MH filter prevents the sampler to move outside of  $\mathcal{P}$  even for an infeasible proposal  $\mathbf{y} \notin \mathcal{P}$ , as  $\alpha(\mathbf{y} | \mathbf{x}) = 0$  in that case. Thus, in principle any unconstrained proposal distribution can be used to

produce samples from constrained densities  $\pi$ . However, using such a proposal distribution quickly grows ineffective when many infeasible  $\mathbf{y} \notin \mathcal{P}$  are proposed and, thus, immediately rejected. Hence, the development and analysis of constrained sampling algorithms has been of great interest (Smith, 1984; Bélisle et al., 1993; Lovász, 1999; Kannan and Narayanan, 2012; Narayanan, 2016; Chen et al., 2017, 2018; Mangoubi and Vishnoi, 2022; Kook et al., 2022; Gatmiry et al., 2024; Srinivasan et al., 2024).

## 2.2 Hit-&-Run Sampler

A simple method, which guarantees the proposal to remain within the constrained domain, is the HR algorithm (Smith, 1984; Bélisle et al., 1993):

---

### Algorithm 1 Hit-&-Run Algorithm

---

- 1: Draw a point  $\mathbf{u}$  uniformly at random from the  $d - 1$  dimensional hypersphere, i.e.  $\|\mathbf{u}\|_2 = 1$ ,
- 2: scale the update with the step size  $\varepsilon$ , i.e.  $\mathbf{v} = \varepsilon\mathbf{u}$ ,
- 3: compute the step size  $\gamma_{\max}$  for which  $\mathbf{x} + \gamma_{\max}\mathbf{v}$  intersects with the constraints,
- 4: draw a step  $\gamma \sim p_{[0, \gamma_{\max}]}$  from the step distribution  $p$  truncated to  $[0, \gamma_{\max}]$ , and
- 5: compute the update  $\mathbf{y} = \mathbf{x} + \gamma\mathbf{v}$ .

---

For brevity, we denote drawing a sample using Alg. 1 as  $\mathbf{y} \sim \text{HR}(\mathbf{x}, \varepsilon^2)$ . The truncated step distribution has density

$$p_{[0, \gamma_{\max}]}(\gamma) = \begin{cases} p(\gamma)/F_p(\gamma), & \text{if } \gamma \in [0, \gamma_{\max}], \\ 0, & \text{else} \end{cases} \quad (3)$$

where  $F_p$  is the cumulative density of the univariate, continuous step distribution  $p$  and  $\gamma_{\max}$  is the intersection with the constraints, i.e.

$$\mathbf{s} := \left( \frac{b_1 - \mathbf{a}_1^\top \mathbf{x}}{\mathbf{a}_1^\top \mathbf{v}}, \dots, \frac{b_m - \mathbf{a}_m^\top \mathbf{x}}{\mathbf{a}_m^\top \mathbf{v}} \right), \quad (4)$$

yielding the largest step size  $\gamma_{\max}$  from  $\mathbf{x}$  along  $\mathbf{v}$  such that  $\mathbf{x} + \gamma_{\max}\mathbf{v} \in \mathcal{P}$ . If  $\mathbf{s}$  has no positive entries, then no constraints lay ahead the direction  $\mathbf{v}$ . In this case, we set  $\gamma_{\max} := \infty$  in which case  $F_p(\infty) := 1$ .

Given  $\gamma_{\max}, p_{[0, \gamma_{\max}]}$  can be sampled using the inverse transform algorithm, if access to the cumulative and inverse cumulative density functions of  $p$  exists. The HR algorithm has, thus, the proposal density

$$q_{\text{HR}}(\mathbf{y} | \mathbf{x}, \varepsilon) = \frac{p_{[0, \gamma_{\max}]}(\|\mathbf{y} - \mathbf{x}\|_2 / \varepsilon)}{(\|\mathbf{y} - \mathbf{x}\|_2 / \varepsilon)^{d-1}} \cdot \frac{\Gamma(d/2)}{2\pi^{d/2}}. \quad (5)$$

Under the mild assumption of  $\text{supp}(p) = \mathbb{R}^+$ , it follows that  $q(\mathbf{y} | \mathbf{x}) > 0$  for any two  $\mathbf{x}, \mathbf{y} \in \mathbb{R}^d$  and, thus, the MH chain with HR proposal distribution converges.

In the limit of  $\gamma_{\max} \rightarrow \infty$  and for the particular choice of  $p$  being the  $\chi_d$  distribution, the HR algorithm draws samples from  $\mathcal{N}(\mathbf{x}, \varepsilon^2 \mathbf{I})$ . This can be seen from decomposing a Gaussian sample  $\boldsymbol{\eta} \sim \mathcal{N}(0, \mathbf{I})$  into its directional and magnitudal components,  $\mathbf{u} = \boldsymbol{\eta} / \|\boldsymbol{\eta}\|$  and  $\gamma = \|\boldsymbol{\eta}\|$ , respectively. Now we observe that the direction  $\mathbf{u} \sim \mathcal{U}_{S^{d-1}}$  follows a uniform distribution on the  $d - 1$  hypersphere  $S^{d-1}$  and the magnitude  $\gamma \sim \chi_d$  follows a  $\chi_d$  distribution.

## 2.3 Higher-Order Sampling Algorithms

In many sampling problems, access to higher-order information of the target density  $\pi$  is available. A well-established method to incorporate first-order information in the sampling process is MALA (Rossky et al., 1978), which proposes new samples

$$\mathbf{y} \sim \mathcal{N}\left(\mathbf{x} + \frac{\varepsilon^2}{2} \nabla \log \varphi(\mathbf{x}), \varepsilon^2 \mathbf{I}\right), \quad (6)$$

before applying the MH filter from Eq. (2). By applying some  $\text{drift } \varepsilon^2 \nabla \log \varphi(\mathbf{x})/2$  towards higher-density regions, MALA often achieves higher sampling efficiency than zeroth-order samplers.

mMALA (Girolami and Calderhead, 2011) extends the original MALA by incorporating second-order information. To this end, mMALA locally preconditions the MALA update using a user-specified metric tensor  $\mathbf{G}(\mathbf{x})$ , which improves

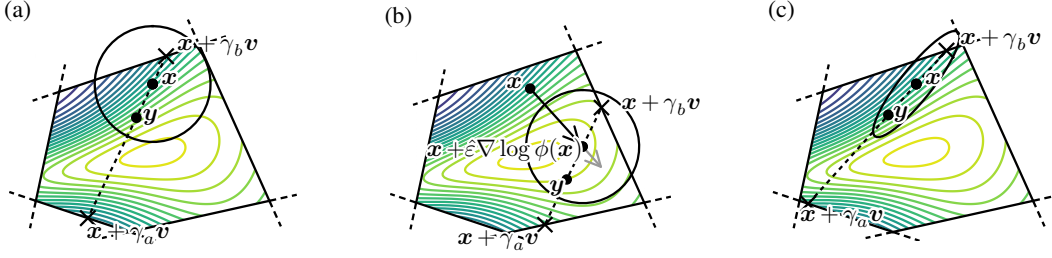


Figure 2: Visualizations of (a) HR, (b) LHR and (c) smHR on a constrained 2-dimensional toy density. A visualization of smLHR is given in Fig. 1.

sampling efficiency for densities admitting locally varying or ill-conditioned curvature. However, mMALA requires the gradient of the metric tensor in order to be the correct Euler-Maruyama discretization of the Riemannian Langevin diffusion on the manifold given by the metric tensor  $\mathcal{G}(\mathbf{x})$ . As this can be computationally expensive, Girolami and Calderhead (2011) also propose a *simplified mMALA* (smMALA), which assumes  $\partial \mathcal{G}(\mathbf{x})/\partial \mathbf{x} = 0$ . The resulting proposal of the simplified algorithm is then

$$\mathbf{y} \sim \mathcal{N}\left(\mathbf{x} + \frac{\varepsilon^2}{2} \mathcal{G}(\mathbf{x})^{-1} \nabla \log \varphi(\mathbf{x}), \varepsilon^2 \mathcal{G}(\mathbf{x})^{-1}\right). \quad (7)$$

Although this results in a “*wrong*” discretization of the Riemannian Langevin diffusion, this is a minor issue in the context of MH sampling, as the MH filter (cf. Eq. (2)) will account for the error and guarantee convergence to the correct target distribution. Indeed, as Girolami and Calderhead (2011) demonstrate empirically, assuming  $\partial \mathcal{G}(\mathbf{x})/\partial \mathbf{x} = 0$  does improve the sampling efficiency per unit of wall clock time, being less efficient yet much faster per sample.

### 3 Higher-Order Hit-&-Run

In this section, we present our approach to combine the zeroth-order HR algorithm with higher-order information. Before delving into technical details, we give a more intuitive overview. Our ideas are motivated by the earlier mentioned observation, that the zeroth-order HR proposal distribution virtually becomes a diagonal Gaussian proposal distribution as the constraints “*move further away*”, though sampled in a manner that decomposes the sample into direction and magnitude components. Now as MALA and smMALA are also just Gaussian proposal distributions, we devise HR-like proposal distributions, which replicate the relationship between HR and diagonal Gaussian proposal distributions, but for the MALA and smMALA.

#### 3.1 Langevin Hit-&-Run

First, we consider the incorporation of gradient information into the HR proposal distribution. A key issue with incorporating gradients into constrained sampling stems from the fact that the gradient, if too large, may quickly push proposals out of  $\mathcal{P}$ , turning them infeasible. Thus, we add a simple clipping mechanism by solving for the intersection of the gradient with the constraints, i.e. we choose  $\kappa$  as the largest positive entry from

$$\kappa := \left( \frac{b - \mathbf{a}_1^\top \mathbf{x}}{\mathbf{a}_1^\top \nabla \log \varphi(\mathbf{x})}, \dots, \frac{b - \mathbf{a}_m^\top \mathbf{x}}{\mathbf{a}_m^\top \nabla \log \varphi(\mathbf{x})} \right). \quad (8)$$

Similarly to Eq. (4), in the case where no positive entries exist in  $\kappa$ , we set  $\kappa := \infty$ , meaning that no constraints are hit when going along the gradient  $\nabla \log \varphi(\mathbf{x})$ . We then clip the drift term at  $\kappa/2$ , i.e. we choose  $\hat{\varepsilon} = \min\{\varepsilon^2/2, \kappa/2\}$  as the gradient step size. Doing so, the drifted mean of our proposal distribution can go at most halfway up until it hits the closest constraint. Using this new clipped step size  $\hat{\varepsilon}$ , we sample our proposal as

$$\mathbf{y} \sim \text{LHR}(\mathbf{x}, \varepsilon^2) := \text{HR}(\mathbf{x} + \hat{\varepsilon} \nabla \log \varphi(\mathbf{x}), \varepsilon^2), \quad (9)$$

which we refer to as the *Langevin Hit-&-Run* (LHR) proposal distribution. We decide to clip at  $\kappa/2$  as getting exactly onto the constraints, i.e. choosing to clip at  $\kappa$ , can have unfavorable effects when computing the intersection  $\gamma_{\max}$ . However, choosing exactly the halfway point  $\kappa/2$  is purely heuristically motivated.

As intended, in the limit of  $\kappa, \gamma_{\max} \rightarrow \infty$ , i.e. when the constraints are “*far away*” from  $\mathbf{x}$ , and for  $p = \chi_d$ , the LHR proposal distribution simplifies to MALA.

### 3.2 Simplified Manifold Langevin Hit-&-Run

Next up, we incorporate curvature information. Ignoring the drift term in smMALA for a moment, smMALA mainly preconditions the Gaussian proposal locally, i.e. let  $\mathbf{L}\mathbf{L}^\top = \mathcal{G}(\mathbf{x})^{-1}$  be the Cholesky factorization of the inverse metric tensor, then – ignoring the drift term – smMALA samples

$$\mathbf{y} = \varepsilon \mathbf{L}^\top \boldsymbol{\eta} = \varepsilon \|\boldsymbol{\eta}\|_2 \mathbf{L}^\top \frac{\boldsymbol{\eta}}{\|\boldsymbol{\eta}\|_2} \quad (10)$$

for  $\boldsymbol{\eta} \sim \mathcal{N}(0, \mathbf{I})$ . Decomposing  $\boldsymbol{\eta}$  into its direction  $\boldsymbol{\eta} / \|\boldsymbol{\eta}\|$  and magnitude  $\|\boldsymbol{\eta}\|$ , the direction follows a uniform distribution on the  $d-1$  hypersphere, i.e.  $\boldsymbol{\eta} / \|\boldsymbol{\eta}\|_2 \sim \mathcal{U}_{S^{d-1}}$ , and the magnitude follows a  $\chi_d$ -distribution, i.e.  $\|\boldsymbol{\eta}\|_2 \sim \chi_d$ . Thus, we can sample  $\mathbf{y}$  using a slight modification of the HR algorithm by preconditioning the directional component  $\boldsymbol{\eta} / \|\boldsymbol{\eta}\|$  by  $\varepsilon \mathbf{L}$ , which – intuitively speaking – results in an HR algorithm that draws the directional component from an ellipsoid rather than a hypersphere. We call this the *elliptical Hit-&-Run* (EHR) algorithm, which we state for some general positive definite covariance matrix  $\Sigma$ :

---

#### Algorithm 2 Elliptical Hit-&-Run Algorithm

---

- 1: Draw a point  $\mathbf{u}$  uniformly at random from the  $d-1$  dimensional hypersphere, i.e.  $\|\mathbf{u}\|_2 = 1$ ,
- 2: **compute the update direction**  $\mathbf{v} = \mathbf{L}^\top \mathbf{u}$ ,
- 3: compute the step size  $\gamma_{\max}$  for which  $\mathbf{x} + \gamma_{\max} \mathbf{v}$  intersects with the constraints,
- 4: draw a step  $\gamma \sim p_{[0, \gamma_{\max}]}^+$  from the step distribution truncated to  $[0, \gamma_{\max}]$ , and
- 5: compute the update  $\mathbf{y} = \mathbf{x} + \gamma \mathbf{v}$ .

---

We denote Alg. 2 in short as  $\mathbf{y} \sim \text{EHR}(\mathbf{x}, \Sigma)$ , for some positive definite matrix  $\Sigma$  with Cholesky factorization  $\Sigma = \mathbf{L}\mathbf{L}^\top$  and assume  $\mathbf{A}, \mathbf{b}, p$  to be given.

Elliptical HR proposals are well-known in the polytope sampling literature (Lovász and Vempala, 2004; Haraldsdóttir et al., 2017; Theorell et al., 2022; Jadebeck et al., 2023), where they are prominently used to apply rounding transformations, which make the polytope more isotropic, but can also be simply considered as a preconditioner to the HR proposal. Unlike in our intended use case, the rounding preconditioner is constant and its contribution to the proposal density cancels out due to symmetry in the MH filter (cf. Eq. (2)). However, MH chains using the EHR proposal distribution with non-constant  $\Sigma(\mathbf{x})$  require the proposal density  $q_{\text{EHR}}(\mathbf{y} | \mathbf{x}, \Sigma(\mathbf{x}))$  in order to compute the MH filter from Eq. (2). To this end, we derive its proposal density, given in the following Lem. 3.1, where we denote the inverse of the transposed Cholesky factor of some symmetric positive definite (s.p.d.)  $\Sigma$  as  $\mathbf{L}^{-\top} := (\mathbf{L}^\top)^{-1}$ . The proof is provided in Sec. A of the appendix.

**Lemma 3.1.** *Assume  $\mathbf{x} \in \mathcal{P}$  and  $\Sigma$  s.p.d., then for  $\mathbf{y} \sim \text{EHR}(\mathbf{x}, \Sigma)$ ,  $\mathbf{y} \in \mathcal{P}$  and has density*

$$q_{\text{EHR}}(\mathbf{y} | \mathbf{x}, \Sigma) \propto \frac{p_{[0, \gamma_{\max}]}^+(\|\mathbf{L}^{-\top}(\mathbf{y} - \mathbf{x})\|_2)}{\|\mathbf{L}^{-\top}(\mathbf{y} - \mathbf{x})\|_2^{d-1} |\det \mathbf{L}|}. \quad (11)$$

With the EHR and LHR algorithms now at hand, we state the *simplified manifold Langevin Hit-&-Run* (smLHR) proposal as

$$\mathbf{y} \sim \text{smLHR}(\mathbf{x}, \varepsilon^2) := \text{EHR}(\mathbf{x} + \hat{\varepsilon} \mathcal{G}(\mathbf{x})^{-1} \nabla \log \varphi(\mathbf{x}), \varepsilon^2 \mathcal{G}(\mathbf{x})^{-1}),$$

where  $\hat{\varepsilon}$  is the clipped step size as in LHR, but for the natural gradient  $\mathcal{G}(\mathbf{x})^{-1} \nabla \log \varphi(\mathbf{x})$ .

We further consider the *simplified manifold Hit-&-Run* (smHR), which omits the gradient step of LHR and only retains the elliptical preconditioning component of smLHR

$$\mathbf{y} \sim \text{smHR}(\mathbf{x}, \varepsilon^2) := \text{EHR}(\mathbf{x}, \varepsilon^2 \mathcal{G}(\mathbf{x})^{-1}). \quad (12)$$

This serves to empirically investigate the influence of the introduced changes to the HR algorithm.

#### 3.2.1 Choice of Metric Tensors

The choice of an appropriate metric is not unique (Girolami and Calderhead, 2011). While the Hessian  $\mathcal{H}(\mathbf{x}) := \nabla^2 \log \varphi(\mathbf{x})$  of the log-density is a natural choice if the latter happens to be concave, it may not be positive definite in the general case, disqualifying it as a metric tensor. In Bayesian inference problems, the sum of the Fisher information

matrix and the Hessian of a strictly log-concave prior yield a meaningful metric (Girolami and Calderhead, 2011). For Riemannian sampling of general densities, the *SoftAbs* (Betancourt, 2013) and the *Monge* metric (Hartmann et al., 2022) have been proposed.

In this work, we additionally test two novel metrics based on the the Hessian of the log-density. The first new metric that we introduce is the squared Hessian metric

$$\mathcal{G}_{\text{sq}}(\mathbf{x}) := \mathcal{H}(\mathbf{x})^\top \mathcal{H}(\mathbf{x}) + \delta \mathbf{I}, \quad (13)$$

which has the favorable property of being positive definite for  $\delta > 0$ , as the squared Hessian term being a Gram matrix is positive semi-definite. However, if the Hessian happens to be locally positive definite, the squared Hessian will apply an undesired second scaling. For this reason, we propose a heuristically motivated approach to adjust the scaling of the squared Hessian metric by taking the element-wise square root of its non-zero entries, i.e. let  $\mathbf{M} := \mathcal{H}(\mathbf{x})^\top \mathcal{H}(\mathbf{x}) \in \mathbb{R}^{d \times d}$  with entries  $m_{ij}$  and  $\text{sgn}$  the sign function, then the new scaled squared Hessian metric becomes

$$\mathcal{G}_{\text{sc}}(\mathbf{x}) := \left( \text{sgn}(m_{ij}) \cdot \sqrt{|m_{ij}|} \right)_{ij} + \delta \mathbf{I}. \quad (14)$$

As the new metric may not be positive definite, we use the diagonal of Eq. (14) as a surrogate metric tensor, if the Cholesky decomposition of the former fails.

**Controlling the Step Size** In practice, the  $\delta$  parameter is not known a priori and typically needs to be tuned using e.g. grid search approaches, as a too large  $\delta$  makes  $\mathcal{G}(\mathbf{x})$  more and more isotropic, effectively reverting the contribution of smLHR. If  $\delta$  is too small, this leads to numerical issues when  $\mathcal{G}(\mathbf{x})$  is not positive definite. Hence,  $\delta$  needs to be tuned for each individual problem, similarly to the step size. However, noting that  $\delta$  also affects the step size and in order to maintain a single tunable hyperparameter, we propose a novel kind of step size parametrization, where we keep  $\varepsilon = 1$  fixed and instead only tune  $\delta$ . In order to keep this approach of controlling the step size comparable to the “classical” one, we reparametrize  $\delta = \lambda^{-2}$  and consider  $\lambda$  the tunable hyperparameter. To distinguish the two approaches, we refer to the algorithms with fixed  $\delta$  as smMALA $_{\varepsilon}$ , smHR $_{\varepsilon}$ , and smLHR $_{\varepsilon}$ , and those that fix  $\varepsilon = 1$  as smMALA $_{\delta}$ , smHR $_{\delta}$  and smLHR $_{\delta}$ . Note that we can apply the  $\delta$ -parametrization to general metrics  $\mathcal{G}(\mathbf{x})$  using  $\hat{\mathcal{G}}(\mathbf{x}) := \mathcal{G}(\mathbf{x}) + \delta \mathbf{I}$  as metric instead. We evaluate both approaches experimentally in Sec. 5.

### 3.3 Convergence Analysis

We state the convergence of our algorithms under the following mild assumption in Thm. 3.2:

- (A1) The state space  $\mathcal{P} \subseteq \mathbb{R}^d$  is convex,
- (A2)  $p$  is positive and continuous on  $\mathbb{R}^+$ , and
- (A3)  $\pi$  is finite and twice continuously differentiable on  $\mathcal{P}$ .

**Theorem 3.2.** Let  $P_{\text{LHR}}, P_{\text{smHR}}, P_{\text{smLHR}}$  be the MH kernels (cf. Eq. (19)) with proposal distributions LHR, smHR, smLHR, respectively. Under assumptions A1–3, for  $\pi$ -almost all  $\mathbf{x}$

$$\|P^n(\mathbf{x}, \cdot) - \pi(\cdot)\|_{\text{TV}} \rightarrow 0, \quad \text{as } n \rightarrow \infty, \quad (15)$$

and for  $P$  being any of  $P_{\text{LHR}}, P_{\text{smHR}}, P_{\text{smLHR}}$ .

A proof is provided in Sec. A in the appendix, here we give a sketch of our argument. Following Nummeling (1984, Theorem 3.7(i) & Prop. 6.3) and Tierney (1994, Theorem 1), any  $\pi$ -irreducible, aperiodic Markov chain with invariant measure  $\pi$  converges in total variation for  $\pi$ -almost all  $\mathbf{x} \in \mathcal{P}$ . However, since the MH chain has  $\pi$  as its invariant measure by construction (Roberts and Rosenthal, 2004, Prop. 1 & 2), it remains to show  $\pi$ -irreducibility and aperiodicity. Aperiodicity follows from the finiteness of  $\pi$  and  $\pi$ -irreducibility of the MH chain (Roberts and Rosenthal, 2004, Running Example). A sufficient condition for  $\pi$ -irreducibility is positivity and continuity of the proposal density on  $\text{supp}(\pi) = \mathcal{P}$  (Robert and Casella, 2004, Eq. (7.5)). For Eq. (11), both requirements follow from assumptions (A1–2) and an additional assumption of  $\Sigma$  being s.p.d. Note that  $\Sigma$  being s.p.d. lies in the responsibility of the practitioner. Since our clipped gradient step does not violate the assumption of  $\mathbf{x} \in \mathcal{P}$  by construction, Thm. A.1 remains valid.

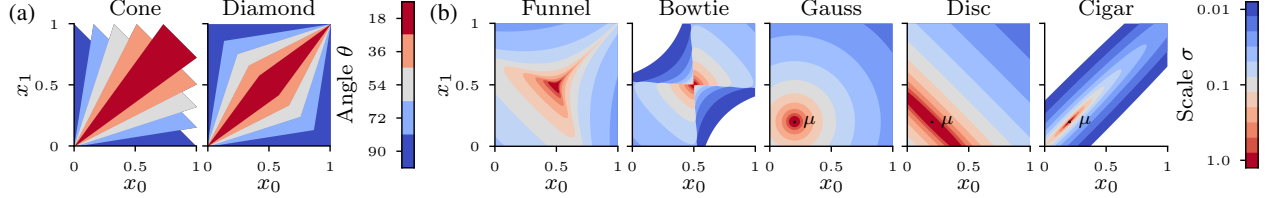


Figure 3: Two-dimensional, exemplary visualizations of the (a) polytopes and (b) densities under consideration, as well as the effect of the respective scale  $\sigma$  and angle  $\theta$  parameters. The mode of the Gaussian densities is controlled by  $\mu$  along the  $(1, \dots, 1)$  axis.

## 4 Related Work

Most work on linearly constrained sampling focuses on uniform densities. Smith (1984) introduced polytope-adapted HR. Berbee et al. (1987) combined HR with Gibbs sampling, also known as Coordinate HR, which was shown to be fast and reliable for uniform sampling, both empirically (Emiris and Fisikopoulos, 2013) and theoretically (Laddha and Vempala, 2022). Moreover, preconditioning (Haraldsdóttir et al., 2017) and thinning (Jadebeck et al., 2023) to minimize cost per sample were shown to further improve performance. Alternatives to HR incorporate linear constraints using local preconditioning based on the Hessian of a barrier function. For example, *Dikin* walk uses the log-barrier (Kannan and Narayanan, 2012) and *Vaidya* walk uses volumetric log-barrier (Chen et al., 2017). Reflection-based approaches also exist (Gryazina and Polyak, 2012).

Apart from uniform sampling, research has mainly explored log-concave distributions. Existing uniform samplers have been transformed into non-uniform ones using the MH filter and were used to sample Gaussian distributions for polytope volume estimation (Cousins and Vempala, 2015; Emiris and Fisikopoulos, 2018). Implementations for MH-based constrained sampling were provided by Jadebeck et al. (2021) & Paul et al. (2024). The first methods to incorporate first-order information into non-uniform constrained sampling were HMC methods, which use the gradient of their target distribution. To address constraints, these methods modify the underlying Hamiltonian dynamics: Kook et al. (2022) and Noble et al. (2023) integrated penalty terms to slow down particles in proximity to the boundary, while Chalkis et al. (2023) introduced a reflection mechanism on the boundaries. These approaches were benchmarked numerically only for truncated Gaussian or uniform target densities.

Based on Girolami and Calderhead (2011) and Kook and Vempala (2024), Srinivasan et al. (2024) propose the MAPLA, a first-order sampler for general distributions on convex domains. MAPLA can be understood as a smMALA variant, which uses the log-barrier's Hessian as metric tensor, preventing second-order information of the log-density from being easily integrated.

## 5 Experiments

We benchmark our algorithms experimentally on synthetic constrained densities with varying curvature or ill-conditioned covariance, as well as on real-world examples from the field of Bayesian  $^{13}\text{C}$  metabolic flux analysis (Theorell et al., 2017). All algorithms were implemented in `blackjax` (Cabezas et al., 2024). We used `jax` (Bradbury et al., 2018) to compute gradients and Hessians of the synthetic densities. For the  $^{13}\text{C}$ -MFA problems, we used the simulation software `13CFLUX` (Stratmann et al., 2025), which also provides gradient and Fisher information computations. Our `blackjax` fork is publicly available at <https://github.com/ripaul/blackjax> and the code for our experiments and figures at <https://github.com/ripaul/manifold-hit-and-run>. All experiments are replicated using four different random seeds.

### 5.1 Synthetic Densities

**Problem Setup** For our constrained densities, we “placed” unconstrained densities in two different kinds of polytopes, which we refer to as *cone* and *diamond*. Both polytopes are parametrized by an angle parameter  $\theta \in (0^\circ, 90^\circ]$  controlling its narrowness. In all cases, the constructed polytope is contained within the  $[0, 1]^d$  box. We visualize this in Fig. 3a, more details including the generalization of our polytopes to higher dimensions are provided in Sec. B in the appendix.

As densities we consider a slight modification of Neal’s *funnel* (Neal, 2003), a *bowtie* distribution and a total of six Gaussians with isotropic and anisotropic covariance structures and two different locations of the mean, such that the mode is once contained within the polytope ( $\mu = 0.5$ ) and once located on the polytope’s border ( $\mu = 0$ ). Bowtie and

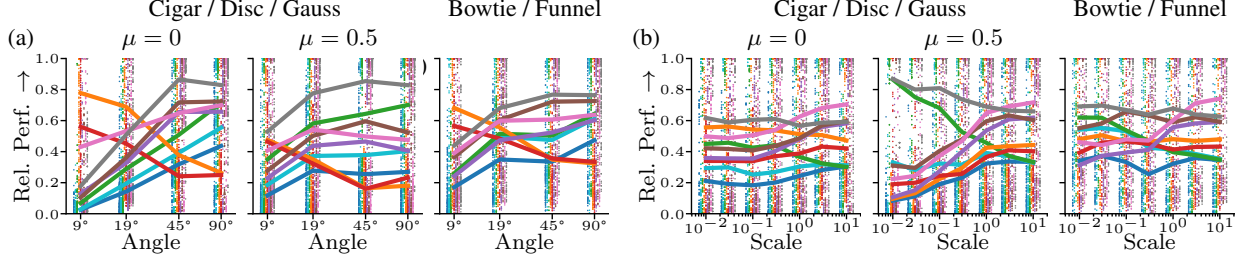


Figure 4: Relative performance of the tested samplers on our benchmark problems as described in Sec. 5. Individual dots show relative performance of individual sampling runs, the solid lines show average relative performance across all problems. Algorithms shown are RWMH—, MALA—, smMALA $_{\delta}$ —, Dikin—, MAPLA—, HR—, LHR—, smHR $_{\delta}$ —, and smLHR $_{\delta}$ —.

funnel are shifted such that their mode is contained within the polytope. A visualization is given in Fig. 3b, more details are provided in Sec. B in the appendix. Moreover, we introduce a scaling parameter  $\sigma$ , which allows to control how close the densities’ high-probability region is to the constraints. That is, if the mode is not located at the polytope’s border, then for small  $\sigma$  the target distribution may be far enough from the constraints to consider the problem effectively unconstrained, whereas for larger  $\sigma$  the target distribution approaches a uniform distribution on  $\mathcal{P}$ .

Finally, for our benchmark, we build our set of problems as the Cartesian product of our eight different densities at log-uniformly chosen scales  $\sigma = 10^{-2}, 10^{-1.5}, \dots, 10^1$  restricted to our two kinds of polytopes, parametrized with angles  $\theta = 9^\circ, 19^\circ, 45^\circ, 90^\circ$  and for dimensions  $d = 2, 4, 8, 16, 32$ , resulting in 2240 different test problems.

**Evaluation** Our main criteria for the evaluation of our algorithms are the L1 error of the joint marginal distribution across the first two dimensions and the minimal marginal effective sample size (minESS), similar to Biron-Lattes et al. (2024). For the former, we ran large-scale MCMC simulations using samplers from the toolbox *hopsy* (Paul et al., 2024) to generate “*ground-truth*” marginal distributions. L1 error is then simply computed across the 2D histograms. We give more details in Sec. B.1 in the appendix.

Since the achievable minESS depends strongly on the problem at hand, we consider the relative performance of an algorithm for every problem as the ratio between its achieved average minESS and the highest achieved average minESS across replicates on the same problem.

We perform a log-uniform grid search of the step size parameter for each algorithm under consideration, and always report results for the step size achieving the smallest L1 error. We test a Gaussian random walk MH sampler (RWMH), MALA, smMALA, Dikin, MAPLA, HR and our introduced algorithms LHR $_{\varepsilon}$ , smHR $_{\varepsilon}$  and smLHR $_{\varepsilon}$ , as well as LHR $_{\delta}$ , smHR $_{\delta}$  and smLHR $_{\delta}$ . For all HR variants, we choose  $p$  to be a half-normal distribution which moment-matches a  $\chi_d$  distribution, as using a  $\chi_d$  distribution is numerically expensive. For the manifold samplers, we use the Hessian as metric tensor for all Gaussian targets and test the SoftAbs (Betancourt, 2013), Monge (Hartmann et al., 2022), squared and scaled squared Hessian metrics from Eq. (13) & Eq. (14), respectively, for the bowtie and funnel densities. For each experiment we run four chains, drawing 20 000  $\cdot d$  samples each and thinning them down to 20 000 to reduce the memory footprint.

Table 1: Mean L1 error of joint marginals of first and second dimension. Best entries per column are marked in bold.

Sampler	Gauss / Cigar / Disc ( $\mu = 0$ )				Gauss / Cigar / Disc ( $\mu = 0.5$ )				Bowtie / Funnel			
	9°	19°	45°	90°	9°	19°	45°	90°	9°	19°	45°	90°
RWMH—	0.373	0.094	0.046	0.047	0.045	0.043	0.049	0.051	0.05	0.045	0.05	0.052
MALA—	0.374	0.093	0.045	0.045	0.043	0.042	0.047	0.049	0.046	0.043	0.048	0.051
smMALA $_{\delta}$ —	0.366	0.088	0.043	0.044	0.041	0.04	0.045	0.046	0.043	0.04	0.045	0.047
Dikin—	<b>0.028</b>	<b>0.034</b>	0.045	0.049	0.042	0.045	0.051	0.053	<b>0.037</b>	0.043	0.05	0.054
MAPLA—	0.03	0.036	0.047	0.051	0.05	0.05	0.052	0.051	0.04	0.045	0.051	0.055
HR—	0.109	0.039	<b>0.041</b>	0.044	0.039	0.042	0.048	0.049	0.041	0.043	0.049	0.051
LHR—	0.109	0.038	<b>0.041</b>	<b>0.043</b>	0.038	0.04	0.047	0.048	0.04	0.041	0.048	0.05
smHR $_{\delta}$ —	0.078	0.036	<b>0.041</b>	0.044	<b>0.036</b>	0.04	0.046	0.047	0.038	0.04	0.046	0.047
smLHR $_{\delta}$ —	0.103	0.037	<b>0.041</b>	<b>0.043</b>	<b>0.036</b>	<b>0.038</b>	<b>0.044</b>	<b>0.045</b>	<b>0.037</b>	<b>0.038</b>	<b>0.044</b>	<b>0.046</b>

**Results** In Fig. 4a and Fig. 4b, we show relative performance of the samplers as functions of the polytopes’ angle parameter and the densities’ scale parameter, respectively. From Fig. 4a, we observe that Dikin— and MAPLA— perform

Table 2: Results on  $^{13}\text{C}$ -MFA problems Best entries per column are marked in bold.

Sampler	Stationary <i>Spiralus</i>			Instationary <i>Spiralus</i>		
	minESS	minESS/s	$\hat{R}$	minESS	minESS/s	$\hat{R}$
RWMH	0.0337	19.891	1.0052	0.0	0.0	2.4501
MALA	0.0154	4.1845	1.0061	0.0	0.0	$\infty$
smMALA $_{\delta}$	<b>0.8667</b>	<b>149.5027</b>	<b>1.0</b>	0.0014	0.0009	1.0278
Dikin	0.0938	55.5012	1.0011	0.0	0.0	2.5191
MAPLA	0.0231	6.0852	1.0029	0.0	0.0	$\infty$
HR	0.0321	13.6633	1.0031	0.0	0.0	2.4559
LHR	0.0177	3.982	1.0075	0.0	0.0	$\infty$
smHR $_{\delta}$	0.2663	62.3391	1.0001	0.0005	0.0006	1.0335
smLHR $_{\delta}$	0.7936	126.1378	1.0001	<b>0.0091</b>	<b>0.0061</b>	<b>1.0015</b>

particularly well for the more narrow polytopes ( $\theta = 9^\circ, 19^\circ$ ) and for the Gaussian target's with  $\mu = 0$ . For the other problems, we observe notable improvement in performance achieved by our methods LHR, smHR $_{\delta}$ , and smLHR $_{\delta}$ . This also becomes apparent in Table 1, where Dikin and MAPLA achieve lowest sampling error for the Gaussian target's at  $\mu = 0$  and  $\theta = 9^\circ, 19^\circ$ , but are outperformed by our HR variants on all other problems. Our observations are in line with the known issues of HR in ill-conditioned polytopes, namely getting stuck in sharp "corners" (Lovász and Vempala, 2004). Further, as expected, the unconstrained samplers RWMH, MALA, smMALA $_{\delta}$  are consistently outperformed by their HR variants HR, LHR and smLHR $_{\delta}$ . The decrease in performance of the unconstrained samplers is particularly noticeable in Fig. 4b, where the constraints become more influential as the scale parameter increases. Fig. 4b also reveals how gradient information becomes less effective in the more uniform setting, as HR and smHR $_{\delta}$  become competitive and even surpass their gradient-based counterparts LHR and smLHR $_{\delta}$  as the scale parameter increases.

Next, we analyze the effect of our proposed metrics and step size parametrization. For the bowtie and funnel targets, the combination of our scaled squared Hessian metric and the  $\delta$ -parametrization from Sec. 3.2.1 achieves highest average relative performance and lowest average L1 error (cf. Figs. 5a and 6a, respectively) across smMALA $_{\delta}$ , smHR $_{\delta}$ , and smLHR $_{\delta}$ . For the Gaussian targets, we also find that our proposed  $\delta$ -parametrization works better than the classical  $\varepsilon$ -parametrization (cf. Figs. 5b and 6b). We suspect that despite the Hessian metric being arguably an optimal proposal covariance in the unconstrained Gaussian case, it fails to account for the polytope constraints. However, it remains unclear to us as to why making the proposal covariance more isotropic using the  $\delta$ -parametrization apparently improves sampling efficiency in the constrained case.

## 5.2 $^{13}\text{C}$ Metabolic Flux Analysis

We further test our algorithms on two test problems, a stationary and non-stationary *Spiralus* (Wiechert et al., 2015), from Bayesian  $^{13}\text{C}$ -MFA (Theorell et al., 2017), where the likelihood computation requires the solution of a set of ordinary differential equations, which reduces to solving a set of algebraic equations for the stationary case. Moreover, in the stationary case, so-called *pool size* parameters vanish, reducing the sampling problem's dimensionality. Where required, we use the Fisher information as metric tensor. As before, we run four chains, each drawing  $10\,000 \cdot d$  and  $40\,000 \cdot d$  samples for stationary and non-stationary *Spiralus*, respectively, and apply thinning by a factor  $d$ .

Our results are presented in Table 2. For the simpler, 2-dimensional isotopically stationary *Spiralus*, we observe that smMALA $_{\delta}$  yields the best performance, closely followed by smLHR $_{\delta}$ . Interestingly, LHR decreases the performance over HR, whereas smHR $_{\delta}$  improves it, suggesting that curvature information is crucial for this problem. For the 9-dimensional isotopically non-stationary *Spiralus*, which entails non-identifiable as well as non-linearly correlated parameters (cf. Fig. 8), curvature information seems crucial in order to successfully sample this problem, as only smMALA $_{\delta}$ , smHR $_{\delta}$ , and smLHR $_{\delta}$  are able to converge within the given budget. Among these, smLHR $_{\delta}$  performs considerably better than its competitors.

## 6 Conclusion

We propose higher-order HR samplers, which work well for linearly constrained, non-uniform densities, often outperforming the Dikin walk and recently introduced MAPLA in our numerical experiments. This suggests, that the combination of both the higher-order information as well as the strictly constrained HR proposal mechanism are key to improve the sampling efficiency for such problems. Notably, our methods seem more robust to “*how far away*” the constraints are from the target distribution’s high-density region, which a priori may not be clear for any given constrained sampling problem. Similarly to the unconstrained case, we observe that incorporating higher-order information typically improves sampling efficiency. Despite HR being slower than its unconstrained counterparts (cf. Fig. 10) due to added complexity, our isotopically non-stationary  $^{13}\text{C}$ -MFA example underlines that higher sampling efficiency translates into faster sampling when likelihood evaluations are expensive.

**Limitations & Future Work** Given the good performance of MAPLA and the Dikin walk in the “*narrow*” polytopes and HRs weakness in such cases, engineering second-order methods that combine rounding transformations or barrier-based metrics with curvature estimates might strike a balance for even more robust constrained samplers.

While our introduced scaled squared Hessian metric and  $\delta$ -parametrization of the step size for the second-order methods show empirically improved performance, future work needs to investigate whether this is more broadly applicable.

## Acknowledgements

RDP’s & AS’ research is funded by the Helmholtz School for Data Science in Life, Earth, and Energy (HDS-LEE). AS, JFJ, MB & KN are thankful to Wolfgang Wiechert for excellent working conditions. The authors gratefully acknowledge computing time on the supercomputer JURECA (Jülich Supercomputing Centre, 2021) at Forschungszentrum Jülich under grant no. hpcmfa.

## References

Greg Ashton, Noam Bernstein, Johannes Buchner, Xi Chen, Gábor Csányi, Andrew Fowlie, Farhan Feroz, Matthew Griffiths, Will Handley, Michael Habeck, Edward Higson, Michael Hobson, Anthony Lasenby, David Parkinson, Livia B Pártay, Matthew Pitkin, Doris Schneider, Joshua S Speagle, Leah South, John Veitch, Philipp Wacker, David J Wales, and David Yallup. Nested sampling for physical scientists. *Nat. Rev. Methods Primers*, 2(1), May 2022.

Atilim Gunes Baydin, Barak A. Pearlmutter, Alexey Andreyevich Radul, and Jeffrey Mark Siskind. Automatic Differentiation in Machine Learning: a Survey. *Journal of Machine Learning Research*, 18(153):1–43, 2018. ISSN 1533-7928.

Claude J. P. Bélisle, H. Edwin Romeijn, and Robert L. Smith. Hit-and-Run Algorithms for Generating Multivariate Distributions. *Mathematics of Operations Research*, 18(2):255–266, 1993. ISSN 0364-765X. Publisher: INFORMS.

H. C. P. Berbee, C. G. E. Boender, A. H. G. Rinnooy Ran, C. L. Scheffer, R. L. Smith, and J. Telgen. Hit-and-run algorithms for the identification of nonredundant linear inequalities. 37(2):184–207, 1987. ISSN 1436-4646.

Michael Betancourt. A general metric for riemannian manifold hamiltonian monte carlo. In Frank Nielsen and Frédéric Barbaresco, editors, *Geometric Science of Information*, pages 327–334, Berlin, Heidelberg, 2013. Springer Berlin Heidelberg. ISBN 978-3-642-40020-9.

Miguel Biron-Lattes, Nikola Surjanovic, Saifuddin Syed, Trevor Campbell, and Alexandre Bouchard-Cote. autoMALA: Locally adaptive Metropolis-adjusted Langevin algorithm. In *Proceedings of The 27th International Conference on Artificial Intelligence and Statistics*, pages 4600–4608. PMLR, April 2024. ISSN: 2640-3498.

Khushboo Borah Slater, Martin Beyß, Ye Xu, Jim Barber, Catia Costa, Jane Newcombe, Axel Theorell, Melanie J Bailey, Dany J V Beste, Johnjoe McFadden, and Katharina Nöh. One-shot  $^{13}\text{C}^{15}\text{C}$  metabolic flux analysis for simultaneous quantification of carbon and nitrogen flux. *Molecular Systems Biology*, 19(3):e11099, 2023.

James Bradbury, Roy Frostig, Peter Hawkins, Matthew James Johnson, Chris Leary, Dougal Maclaurin, George Necula, Adam Paszke, Jake VanderPlas, Skye Wanderman-Milne, and Qiao Zhang. JAX: composable transformations of Python+NumPy programs, 2018.

Alberto Cabezas, Adrien Corenflos, Junpeng Lao, Rémi Louf, Antoine Carnec, Kaustubh Chaudhari, Reuben Cohn-Gordon, Jeremie Couillon, Wei Deng, Sam Duffield, Gerardo Durán-Martín, Marcin Elantkowski, Dan Foreman-Mackey, Michele Gregori, Carlos Igúaran, Ravin Kumar, Martin Lysy, Kevin Murphy, Juan Camilo Orduz, Karm Patel, Xi Wang, and Rob Zinkov. BlackJAX: Composable Bayesian inference in JAX, February 2024. arXiv:2402.10797 [cs].

Apostolos Chalkis, Vissarion Fisikopoulos, Marios Papachristou, and Elias Tsigaridas. Truncated log-concave sampling with reflective hamiltonian monte carlo. 49(2):1–25, 2023. ISSN 0098-3500, 1557-7295.

Yuansi Chen, Raaz Dwivedi, Martin J. Wainwright, and Bin Yu. Vaidya walk: A sampling algorithm based on the volumetric barrier. In *2017 55th Annual Allerton Conference on Communication, Control, and Computing (Allerton)*, pages 1220–1227, October 2017.

Yuansi Chen, Raaz Dwivedi, Martin J. Wainwright, and Bin Yu. Fast MCMC Sampling Algorithms on Polytopes. *Journal of Machine Learning Research*, 19(55):1–86, 2018. ISSN 1533-7928.

Benjamin Cousins and Santosh Vempala. Bypassing KLS: Gaussian cooling and an  $\alpha^*(n^3)$  volume algorithm. In *Proceedings of the forty-seventh annual ACM symposium on Theory of Computing*, STOC ’15, pages 539–548. Association for Computing Machinery, 2015. ISBN 978-1-4503-3536-2.

Simon Duane, A. D. Kennedy, Brian J. Pendleton, and Duncan Roweth. Hybrid Monte Carlo. *Physics Letters B*, 195(2):216–222, September 1987. ISSN 0370-2693.

Ioannis Z. Emiris and Vissarion Fisikopoulos. Efficient random-walk methods for approximating polytope volume, 2013. version: 1.

Ioannis Z. Emiris and Vissarion Fisikopoulos. Practical polytope volume approximation. 44(4):38:1–38:21, 2018. ISSN 0098-3500.

Anthony V Fiacco and Garth P McCormick. *Nonlinear programming*. Society for Industrial and Applied Mathematics, January 1990.

Khashayar Gatmiry, Jonathan Kelner, and Santosh S. Vempala. Sampling Polytopes with Riemannian HMC: Faster Mixing via the Lewis Weights Barrier. In *Proceedings of Thirty Seventh Conference on Learning Theory*, pages 1796–1881. PMLR, June 2024. ISSN: 2640-3498.

Gabriel Gellner, Kevin McCann, and Alan Hastings. Stable diverse food webs become more common when interactions are more biologically constrained. *Proceedings of the National Academy of Sciences*, 120(31):2017, 2023.

Mark Girolami and Ben Calderhead. Riemann manifold Langevin and Hamiltonian Monte Carlo methods. *Journal of the Royal Statistical Society: Series B (Statistical Methodology)*, 73(2):123–214, 2011. ISSN 1467-9868.

Elena Gryazina and Boris Polyak. Random sampling: Billiard walk algorithm, 2012. version: 2.

Hulda S Haraldsdóttir, Ben Cousins, Ines Thiele, Ronan M.T Fleming, and Santosh Vempala. CHRR: coordinate hit-and-run with rounding for uniform sampling of constraint-based models. *Bioinformatics*, 33(11):1741–1743, June 2017. ISSN 1367-4803.

Marcelo Hartmann, Mark Girolami, and Arto Klami. Lagrangian manifold monte carlo on monge patches. In Gustau Camps-Valls, Francisco J. R. Ruiz, and Isabel Valera, editors, *Proceedings of The 25th International Conference on Artificial Intelligence and Statistics*, volume 151 of *Proceedings of Machine Learning Research*, pages 4764–4781. PMLR, 28–30 Mar 2022.

W. K. Hastings. Monte Carlo Sampling Methods Using Markov Chains and Their Applications. *Biometrika*, 57(1):97–109, 1970. ISSN 0006-3444. Publisher: [Oxford University Press, Biometrika Trust].

Helena A. Herrmann, Beth C. Dyson, Lucy Vass, Giles N. Johnson, and Jean-Marc Schwartz. Flux sampling is a powerful tool to study metabolism under changing environmental conditions. *npj Systems Biology and Applications*, 5(1):32, 2019.

Johann F Jadebeck, Axel Theorell, Samuel Leweke, and Katharina Nöh. HOPS: high-performance library for (non-)uniform sampling of convex-constrained models. *Bioinformatics*, 37(12):1776–1777, July 2021. ISSN 1367-4803, 1367-4811.

Johann F. Jadebeck, Wolfgang Wiechert, and Katharina Nöh. Practical sampling of constraint-based models: Optimized thinning boosts CHRR performance. *PLOS Computational Biology*, 19(8):e1011378, August 2023. ISSN 1553-7358. Publisher: Public Library of Science.

Jülich Supercomputing Centre. JURECA: Data Centric and Booster Modules implementing the Modular Supercomputing Architecture at Jülich Supercomputing Centre. *Journal of large-scale research facilities*, 7(A182), 2021.

Ravindran Kannan and Hariharan Narayanan. Random Walks on Polytopes and an Affine Interior Point Method for Linear Programming. *Mathematics of Operations Research*, 37(1):1–20, February 2012. ISSN 0364-765X. Publisher: INFORMS.

Yunbum Kook and Santosh S. Vempala. Gaussian cooling and dikan walks: The interior-point method for logconcave sampling, 2024.

Yunbum Kook, YinTat Lee, Ruoqi Shen, and Santosh Vempala. Sampling with Riemannian Hamiltonian Monte Carlo in a Constrained Space. October 2022.

Aditi Laddha and Santosh Vempala. Convergence of gibbs sampling: Coordinate hit-and-run mixes fast, 2022.

Krzysztof Łatuszyński and Daniel Rudolf. Convergence of hybrid slice sampling via spectral gap. *Advances in Applied Probability*, 56(4):1440–1466, 2024.

Yifang Li and Sujit K. Ghosh. Efficient sampling methods for truncated multivariate normal and student-t distributions subject to linear inequality constraints. *Journal of Statistical Theory and Practice*, 9(4):712–732, Dec 2015. ISSN 1559-8616.

László Lovász. Hit-and-run mixes fast. *Mathematical Programming*, 86(3):443–461, December 1999. ISSN 1436-4646.

László Lovász and Santosh Vempala. Hit-and-run from a corner. In *Proceedings of the thirty-sixth annual ACM symposium on Theory of computing*, STOC ’04, pages 310–314, New York, NY, USA, June 2004. Association for Computing Machinery. ISBN 978-1-58113-852-8.

László Lovász and Santosh Vempala. Hit-and-run from a corner. *SIAM Journal on Computing*, 35(4):985–1005, 2006.

M. Lubini, M. Sereno, J. Coles, Ph. Jetzer, and P. Saha. Cosmological parameter determination in free-form strong gravitational lens modelling. *Monthly Notices of the Royal Astronomical Society*, 437(3):2461–2470, 2013.

Oren Mangoubi and Nisheeth K. Vishnoi. Sampling from Log-Concave Distributions with Infinity-Distance Guarantees. October 2022.

Nicholas Metropolis, Arianna W. Rosenbluth, Marshall N. Rosenbluth, Augusta H. Teller, and Edward Teller. Equation of State Calculations by Fast Computing Machines. *The Journal of Chemical Physics*, 21(6):1087–1092, June 1953. ISSN 0021-9606, 1089-7690.

Hariharan Narayanan. Randomized interior point methods for sampling and optimization. *The Annals of Applied Probability*, 26(1):597–641, February 2016. ISSN 1050-5164, 2168-8737. Publisher: Institute of Mathematical Statistics.

Radford M. Neal. Slice sampling. *The Annals of Statistics*, 31(3):705–767, June 2003. ISSN 0090-5364, 2168-8966. Publisher: Institute of Mathematical Statistics.

Maxence Noble, Valentin De Bortoli, and Alain Durmus. Unbiased constrained sampling with self-concordant barrier hamiltonian monte carlo, 2023.

Esa Nummelin. *General Irreducible Markov Chains and Non-Negative Operators*. Cambridge Tracts in Mathematics. Cambridge University Press, Cambridge, 1984. ISBN 978-0-521-60494-9.

Richard D Paul, Johann F Jadebeck, Anton Stratmann, Wolfgang Wiechert, and Katharina Nöh. hopsy — a methods marketplace for convex polytope sampling in Python. *Bioinformatics*, 40(7):btae430, July 2024. ISSN 1367-4811.

Christian P. Robert and George Casella. *Monte Carlo Statistical Methods*. Springer Texts in Statistics. Springer, New York, NY, 2004. ISBN 978-1-4419-1939-7 978-1-4757-4145-2.

Gareth O. Roberts and Jeffrey S. Rosenthal. General state space Markov chains and MCMC algorithms. *Probability Surveys*, 1(none):20–71, January 2004. ISSN 1549-5787, 1549-5787. Publisher: Institute of Mathematical Statistics and Bernoulli Society.

P. J. Rossky, J. D. Doll, and H. L. Friedman. Brownian dynamics as smart Monte Carlo simulation. *The Journal of Chemical Physics*, 69(10):4628–4633, November 1978. ISSN 0021-9606.

Robert L. Smith. Efficient Monte Carlo Procedures for Generating Points Uniformly Distributed Over Bounded Regions. *Operations Research*, 32(6):1296–1308, 1984. ISSN 0030-364X. Publisher: INFORMS.

Vishwak Srinivasan, Andre Wibisono, and Ashia C. Wilson. High-accuracy sampling from constrained spaces with the Metropolis-adjusted Preconditioned Langevin Algorithm. In *36th International Conference on Algorithmic Learning Theory*, December 2024.

Anton Stratmann, Martin Beyß, Johann F Jadebeck, Wolfgang Wiechert, and Katharina Nöh. 13CFLUX - third-generation high-performance engine for isotopically (non)stationary  $^{13}\text{C}$  metabolic flux analysis. *Bioinformatics*, 41(12):btaf630, 11 2025. ISSN 1367-4811.

Tommi Tervonen, Gert van Valkenhoef, Nalan Baştürk, and Douwe Postmus. Hit-and-run enables efficient weight generation for simulation-based multiple criteria decision analysis. *European Journal of Operational Research*, 224(3):552–559, 2013. ISSN 0377-2217.

Axel Theorell and Katharina Nöh. Reversible jump mcmc for multi-model inference in metabolic flux analysis. *Bioinformatics*, 36(1):232–240, 06 2019. ISSN 1367-4803.

Axel Theorell, Samuel Leweke, Wolfgang Wiechert, and Katharina Nöh. To be certain about the uncertainty: Bayesian statistics for  $^{13}\text{C}$  metabolic flux analysis. *Biotechnology and Bioengineering*, 114(11):2668–2684, 2017. ISSN 1097-0290.

Axel Theorell, Johann F Jadebeck, Katharina Nöh, and Jörg Stelling. PolyRound: polytope rounding for random sampling in metabolic networks. *Bioinformatics*, 38(2):566–567, January 2022. ISSN 1367-4803.

Luke Tierney. Markov Chains for Exploring Posterior Distributions. *The Annals of Statistics*, 22(4):1701–1728, 1994. ISSN 0090-5364. Publisher: Institute of Mathematical Statistics.

Wolfgang Wiechert, Sebastian Niedenführ, and Katharina Nöh. *A Primer to  $^{13}\text{C}$  Metabolic Flux Analysis*, chapter 5, pages 97–142. John Wiley & Sons, Ltd, 2015. ISBN 9783527697441.

## A Missing Proofs

In this section we present missing proofs for Thm. 3.1 and Thm. 3.2. We begin with a proof of the EHR density (cf. Eq. (11)):

*Proof of Thm. 3.1.* Let  $\Delta := \mathbf{y} - \mathbf{x} = \gamma \mathbf{v}$ , then step size and direction on the ellipsoid are recovered as  $\|\mathbf{L}^{-\top} \Delta\|_2 = \gamma \|\mathbf{L}^{-\top} \mathbf{L}^\top \mathbf{u}\|_2 = \gamma$ , since  $\|\mathbf{u}\|_2 = 1$  and  $\mathbf{v} = \Delta/\gamma$ . This transformation is a change of basis from Cartesian to spherical coordinates with differential volume  $d\Delta = |\det \mathbf{L}| \cdot \gamma^{d-1} \cdot d\gamma d\omega$ , thus, the Jacobian determinant of the bijection  $\Delta = \gamma \mathbf{L}^\top \mathbf{u}$  is

$$\left| \frac{\partial \Delta}{\partial(\gamma, \mathbf{u})} \right| = |\det \mathbf{L}| \cdot \gamma^{d-1} \quad (16)$$

and by the inverse function theorem, the Jacobian determinant of the inverse map is the inverse of the Jacobian determinant of the forward map, i.e.

$$\left| \frac{\partial(\gamma, \mathbf{u})}{\partial \Delta} \right| = \left| \frac{\partial \Delta}{\partial(\gamma, \mathbf{u})} \right|^{-1} = \frac{1}{|\det \mathbf{L}| \cdot \gamma^{d-1}}. \quad (17)$$

Now by transform of random variables, we have that

$$q_{\text{HR}}(\mathbf{y} | \mathbf{x}, \Sigma) = p(\gamma, \mathbf{u} | \mathbf{x}, \Sigma) \left| \frac{\partial(\gamma, \mathbf{u})}{\partial \Delta} \right| = \frac{p(\gamma | \mathbf{u}, \mathbf{x}, \Sigma) p(\mathbf{u})}{|\det \mathbf{L}| \cdot \gamma^{d-1}} = \frac{p(\gamma | \mathbf{u}, \mathbf{x}, \Sigma)}{|\det \mathbf{L}| \cdot \gamma^{d-1}} \frac{\Gamma(d/2)}{2\pi^{d/2}}, \quad (18)$$

where the last equality follows from  $p(\mathbf{u}) = 1/A_{d-1}$  being the uniform distribution on the surface of the  $d-1$  hypersphere, which has area  $A_{d-1} = 2\pi^{d/2}/\Gamma(d/2)$ . Finally,  $p(\gamma | \mathbf{u}, \mathbf{x}, \Sigma)$  is just the truncated step density  $p_{[0, \gamma_{\max}]}(\gamma)$  as defined in Alg. 2. Recalling our earlier definitions, we have that  $\gamma = \|\mathbf{L}^{-\top}(\mathbf{y} - \mathbf{x})\|_2$ , thus recovering Eq. (11).  $\square$

Next, we fill out the technical details of our sketched convergence argument from Sec. 3.3. Let

$$P(\mathbf{x}, \mathbf{y}) := \alpha(\mathbf{y} | \mathbf{x}) q(\mathbf{y} | \mathbf{x}) + (1 - r(\mathbf{x})) \delta_{\mathbf{x}}(\mathbf{y}), \quad \text{with} \quad r(\mathbf{x}) := \int_{\mathcal{P}} \alpha(\mathbf{z} | \mathbf{x}) q(\mathbf{z} | \mathbf{x}) d\mathbf{z} \quad (19)$$

be the *Metropolis kernel*, where  $\delta_{\mathbf{x}}(\mathbf{y})$  is the Dirac measure on  $\mathbf{x}$ ,  $\alpha(\mathbf{y} | \mathbf{x})$  is the MH filter (cf. Eq. (2)) and  $q(\cdot | \mathbf{x})$  is some proposal distribution conditionally on  $\mathbf{x}$ . Moreover,

$$P^n(\mathbf{x}, \mathbf{y}) = \int_{\mathcal{P}} P^{n-1}(\mathbf{x}, \mathbf{z}) P(\mathbf{z}, \mathbf{y}) d\mathbf{z} \quad (20)$$

is the recursively defined  $n$ -step kernel with  $P^0(\mathbf{x}, \mathbf{y}) := \delta_{\mathbf{x}}(\mathbf{y})$ .

As discussed in Sec. 3.3, for a positive proposal distribution, i.e.  $q(\mathbf{y} | \mathbf{x}) > 0$  for any two  $\mathbf{x}, \mathbf{y} \in \mathcal{P}$ , convergence of the  $n$ -step kernel to the desired target distribution is given by standard arguments under assumption (A3), as positivity then implies  $\pi$ -irreducibility and aperiodicity, and thus convergence (Roberts and Rosenthal, 2004). Therefore, it only remains to show that our algorithms' proposal density is indeed positive. To show this, we first prove that  $q_{\text{EHR}}(\cdot | \mathbf{x})$  is positive for any  $\mathbf{x} \in \mathcal{P}$  under assumptions A1–2 and additionally if  $\Sigma$  is positive definite.

**Lemma A.1.** *Let  $p$  be positive and continuous on  $\mathbb{R}$ ,  $\Sigma = \mathbf{L}\mathbf{L}^\top$  s.p.d. Then,*

$$q_{\text{EHR}}(\mathbf{y} | \mathbf{x}, \Sigma) = \frac{p_{[0, \gamma_{\max}]}(\|\mathbf{L}^{-\top}(\mathbf{y} - \mathbf{x})\|_2)}{\|\mathbf{L}^{-\top}(\mathbf{y} - \mathbf{x})\|_2^{d-1} |\det \mathbf{L}|} \cdot \frac{\Gamma(d/2)}{2\pi^{d/2}}$$

*is positive and continuous for all  $\mathbf{x}, \mathbf{y} \in \mathcal{P}$  with  $\mathbf{x} \neq \mathbf{y}$ .*

*Proof.* We prove positivity by contradiction. Assume  $\mathbf{y} \in \mathcal{P}$  with  $q_{\text{EHR}}(\mathbf{y} | \mathbf{x}, \Sigma) = 0$ . By regularity of  $\Sigma = \mathbf{L}\mathbf{L}^\top$ , we always find  $\mathbf{u} = \mathbf{L}^{-\top}(\mathbf{y} - \mathbf{x})/\gamma$  such that  $\mathbf{y} = \gamma \mathbf{L}\mathbf{u} + \mathbf{x}$  for some  $\gamma$ . By convexity, we have that  $\gamma \in [0, \gamma_{\max}]$ , however by positivity of  $p$  on  $\mathbb{R}$ , it follows that  $p_{[\gamma_a, \gamma_b]}(\gamma) > 0$  and thus  $q_{\text{EHR}}(\mathbf{y} | \mathbf{x}, \Sigma) > 0$ , which is a contradiction. Finally,  $q_{\text{EHR}}(\mathbf{y} | \mathbf{x}, \Sigma)$  is a chain of continuous functions and thereby continuous itself.  $\square$

Given Thm. A.1, we now state the proof of Thm. 3.2.

*Proof of Thm. 3.2.* By Thm. A.1 and the argument provided in Sec. 3.3, convergence of any of our three algorithms follows if we show that  $\Sigma$  is s.p.d. and the clipped gradient step remains within  $\mathcal{P}$ .

LHR: Since  $\text{LHR}(\mathbf{x}, \varepsilon^2) = \text{EHR}(\cdot | \mathbf{x} + \hat{\varepsilon} \nabla \log \varphi(\mathbf{x}), \varepsilon^2 I)$ , we have that  $\varepsilon^2 I$  is s.p.d. for  $\varepsilon > 0$  and it only remains to show that  $\mathbf{x} + \hat{\varepsilon} \nabla \log \varphi(\mathbf{x}) \in \mathcal{P}$ , which however follows from convexity since  $\mathbf{x}, \mathbf{x} + \kappa \nabla \log \varphi(\mathbf{x}) \in \mathcal{P}$  and  $\hat{\varepsilon} \in (0, \kappa/2]$ . Therefore,  $P_{\text{LHR}}$  converges in total variation distance to the desired target distribution.

smHR: For  $\text{smHR}(\mathbf{x}, \varepsilon^2) = \text{EHR}(\cdot | \mathbf{x}, \varepsilon^2 \mathcal{G}(\mathbf{x})^{-1})$  it is only necessary to show that  $\mathcal{G}(\mathbf{x})$  is s.p.d., as the inverse of an s.p.d. matrix is itself s.p.d., which however follows from construction in Eq. (14) and for  $\delta$  large enough. Therefore,  $P_{\text{smHR}}$  converges in total variation distance to the desired target distribution.

smLHR: Convergence of  $P_{\text{smLHR}}$  follows directly from that of  $P_{\text{LHR}}$  and  $P_{\text{smHR}}$ .  $\square$

## B Experiment Details

### B.1 Ground Truth Sampling

We collect “ground truth” samples from our synthetic densities by running large MCMC simulations using the HR sampler from the toolbox `hopsy`. For each problem, we run four parallel chains. For the bowtie and funnel, we draw  $1\,000\,000 \cdot d \log_2 d$  samples using the HR sampler with a Gaussian step distribution with step size being the scale parameter  $\sigma$  of the respective target. For the Gaussian targets, we draw  $100\,000 \cdot d \log_2 d$  samples using the truncated Gaussian sampler (Li and Ghosh, 2015).

### B.2 Synthetic Densities

**Densities** As densities we consider Neal’s funnel (Neal, 2003), with  $x_1 \sim \mathcal{N}(0, 9)$ ,  $x_i \sim \mathcal{N}(0, e^{x_1})$ ,  $i = 2, \dots, d$ , a *bowtie* distribution with  $x_1 \sim \mathcal{N}(0, 1)$ ,  $x_i \sim \mathcal{N}(0, x_1^2/4 + 0.1)$ ,  $i = 2, \dots, d$ , and six differently parametrized Gaussians: an isotropic, zero-centered Gaussian, a disc-like zero-centered Gaussian with marginal variances  $\sigma_1^2 = 1/100$  and  $\sigma_i = 1$ ,  $i = 1, \dots, d$ , and a cigar-like zero-centered Gaussian with marginal variances  $\sigma_1^2 = 1$  and  $\sigma_i = 1/100$ ,  $i = 1, \dots, d$ . We consider two different versions of those three Gaussian targets, where the mode is either located at the origin or on the midpoint between origin and the intersection of the  $(1, \dots, 1)$  vector with the polytope borders, which guarantees that the mode will be contained in the polytope  $\mathcal{P}$ . Moreover, we apply a multivariate location-scale transformation

$$\varphi(\mathbf{x}) := \varphi_0 \left( \mathbf{Q}^\top \left( \frac{\mathbf{x} - \mathbf{m}}{\sigma} \right) \right), \quad (21)$$

where  $\mathbf{Q}^\top$  rotates the  $(1, 0, \dots, 0)$  vector to  $(1, \dots, 1)$ . For the funnel and bowtie distributions,  $\mathbf{m}$  is determined as the halfway point between the origin and the intersection of the  $(1, \dots, 1)$  vector with the polytope, which is supposed to keep the “characteristic” regions of the density inside the polytope. For the Gaussian distributions, we set  $\mathbf{m} = 0$ .

**Polytopes** The *cone* is constructed as a simplex with tilted sides and a scaled constraint in Eq. (23), which bounds the polytope within the  $[0, 1]^d$  box:

$$\cos(\theta) \cdot x_i - \sin(\theta) \cdot x_j \leq 0 \quad \text{for any two different } i, j = 1, \dots, d, \quad (22)$$

$$\sum_{i=1}^d x_i \leq \frac{\cos(\theta)}{\sin(\theta)} + 1. \quad (23)$$

The *diamond* is constructed as a  $[0, 1]^d$  whose sides are also tilted and scaled such that the resulting parallelogram is contained in the  $[0, 1]^d$  box:

$$\cos(\theta) \cdot x_i - \sin(\theta) \cdot x_j \leq 0 \quad \text{for any two different } i, j = 1, \dots, d, \quad (24)$$

$$-\cos(\theta) \cdot x_i + \sin(\theta) \cdot x_j \leq \sin(\theta) - \cos(\theta) \quad \text{for any two different } i, j = 1, \dots, d. \quad (25)$$

## C Additional Figures & Tables

We provide additional figures. In Fig. 6a & 6b, we provide L1 error results based on the used metric. In Fig. 7 & 8, we provide pair plots of the two-dimensional marginal parameter posterior distributions, sampled using our smLHR $_\delta$

sampler. Fig. 9, 10 & 11 further dissect the performance of the various tested samplers. For better accessibility, we provide these results also in tabular format.

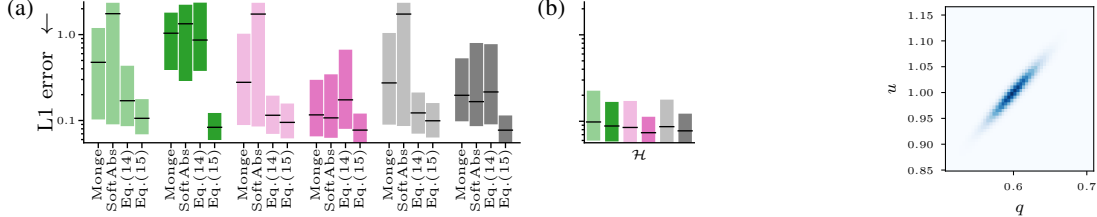


Figure 6: L1 error of smMALA $_{\varepsilon}$ , smMALA $_{\delta}$ , smHR $_{\varepsilon}$ , smHR $_{\delta}$ , smLHR $_{\varepsilon}$  & smLHR $_{\delta}$  using (a) different choices of metric for the bowtie and funnel, and (b) on the Gaussian targets. Colored bars show the 25%

Figure 7: Pair plot of parameter posterior distribution of the isotopically stationary *Spiralus* model, sampled using our smLHR $_{\delta}$  method. Parameter names follow Wiechert et al. (2015).

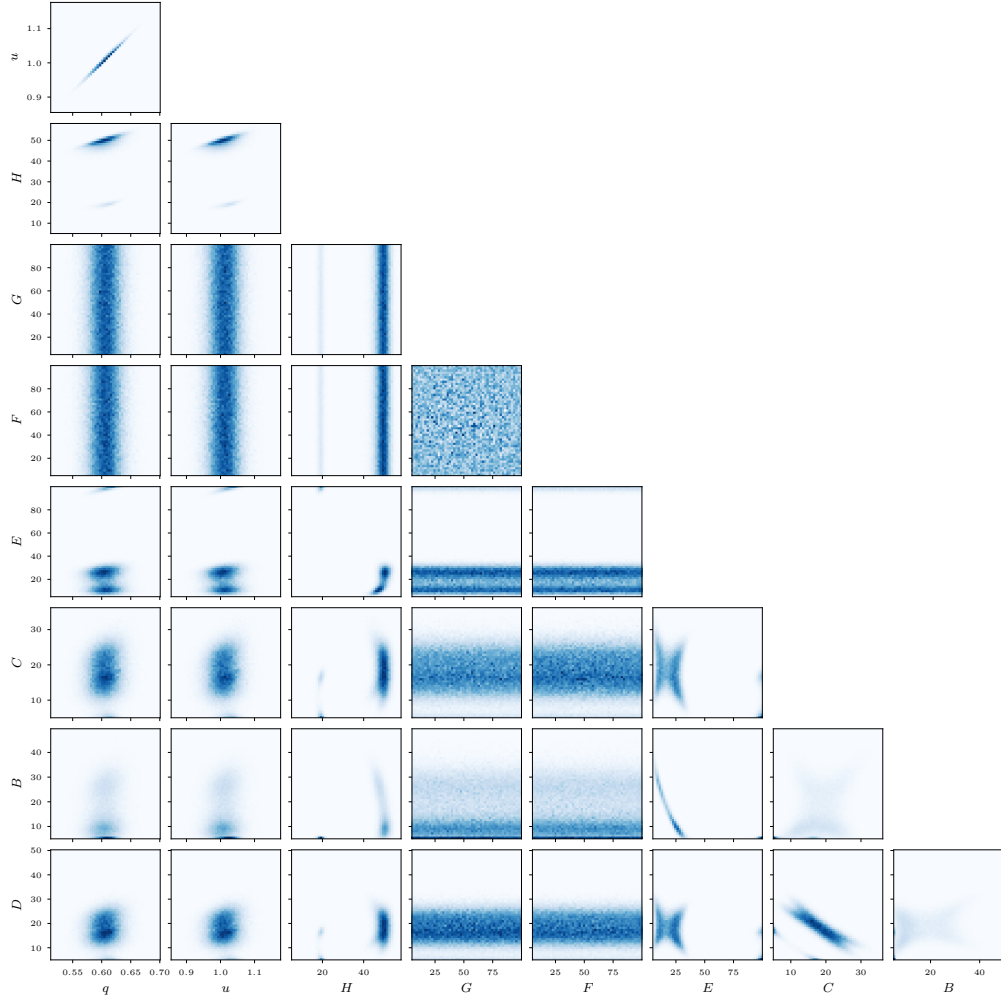


Figure 8: Pair plot of parameter posterior distribution of the isotopically non-stationary *Spiralus* model, sampled using our smLHR $_{\delta}$  method. Parameter names follow Wiechert et al. (2015).

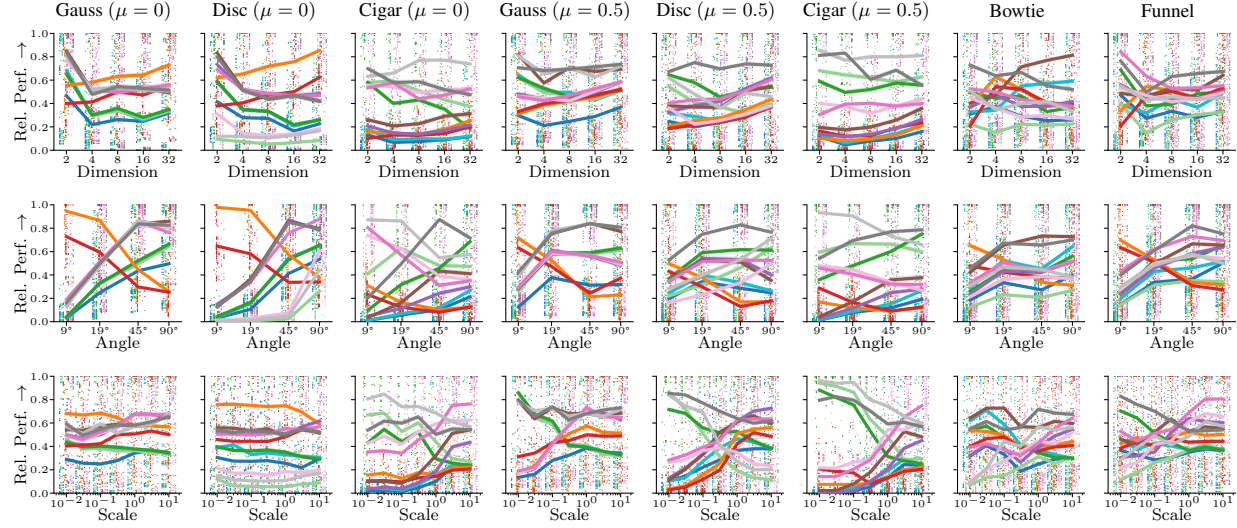


Figure 9: Detailed presentation of relative performance of the tested samplers on our benchmark problems as described in Sec. 5. Individual dots show relative performance of individual sampling runs, the solid lines show average relative performance across all problems. Algorithms shown are RWMH (blue line), MALA (cyan line), smMALA $_{\varepsilon}$  (green line), smMALA $_{\delta}$  (green line), Dikin (orange line), MAPLA (red line), HR (purple line), LHR (brown line), smHR $_{\varepsilon}$  (pink line), smHR $_{\delta}$  (pink line), smLHR $_{\varepsilon}$  (grey line), and smLHR $_{\delta}$  (grey line).

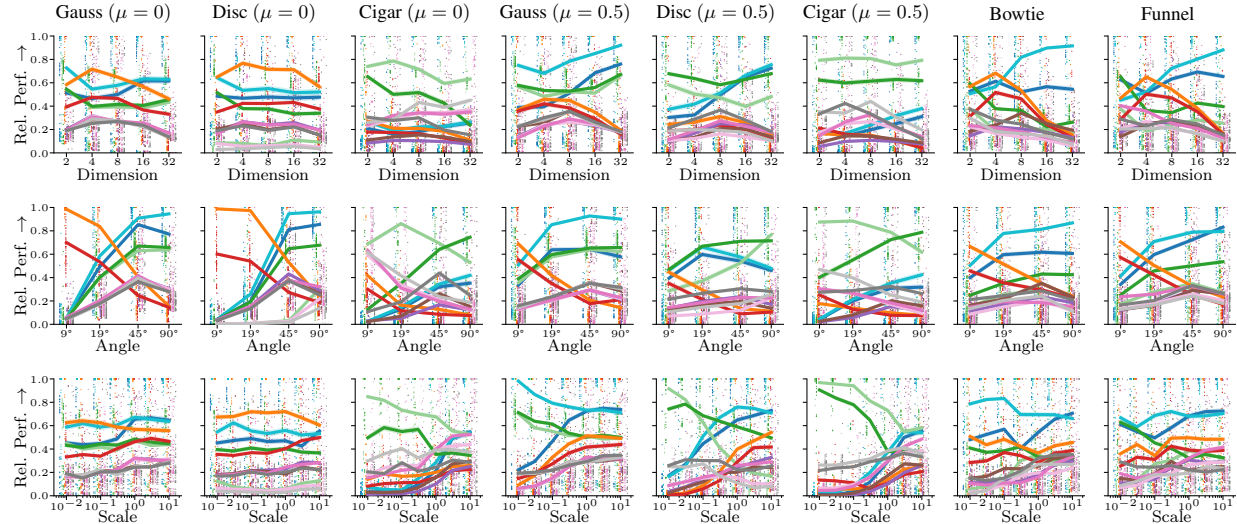


Figure 10: Detailed presentation of relative performance based on minESS/s of the tested samplers on our benchmark problems as described in Sec. 5. Individual dots show relative performance of individual sampling runs, the solid lines show average relative performance across all problems. Algorithms shown are RWMH (blue line), MALA (cyan line), smMALA $_{\varepsilon}$  (green line), smMALA $_{\delta}$  (green line), Dikin (orange line), MAPLA (red line), HR (purple line), LHR (brown line), smHR $_{\varepsilon}$  (pink line), smHR $_{\delta}$  (pink line), smLHR $_{\varepsilon}$  (grey line), and smLHR $_{\delta}$  (grey line).

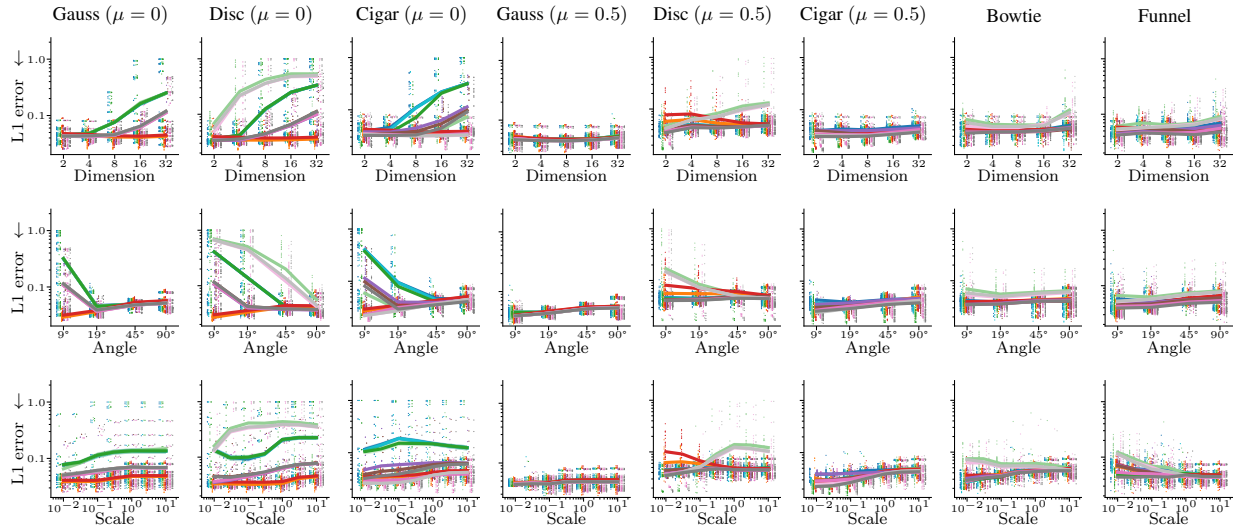


Figure 11: Detailed presentation of average L1 error of the tested samplers on our benchmark problems as described in Sec. 5. Individual dots show relative performance of individual sampling runs, the solid lines show average relative performance across all problems. Algorithms shown are RWMH, MALA, smMALA $_{\varepsilon}$ , smMALA $_{\delta}$ , Dikin, MAPLA, HR, LHR, smHR $_{\varepsilon}$ , smHR $_{\delta}$ , smLHR $_{\varepsilon}$ , and smLHR $_{\delta}$ .

Table 3: Average relative performance of the tested samplers across dimensions as presented as solid lines in Fig. 9.

Sampler	Target	2	4	8	16	32	2	4	8	16	32	2	4	8	16	32	2	4	8	16	32	2	4	8	16	32	2	4	8	16	32	2	4	8	16	32	
RWMH	$\mathbb{R}^d$	0.13	0.067	0.074	0.09	0.116	0.144	0.272	0.357	0.447	0.536	0.247	0.338	0.427	0.517	0.607	0.077	0.101	0.159	0.210	0.254	0.29	0.368	0.429	0.487	0.545	0.611	0.677	0.733	0.793	0.854	0.918	0.934	0.973	0.982	0.993	0.999
MALA	$\mathbb{R}^d$	0.176	0.089	0.101	0.096	0.122	0.152	0.207	0.261	0.326	0.383	0.247	0.337	0.424	0.513	0.602	0.143	0.212	0.317	0.429	0.521	0.607	0.694	0.749	0.811	0.871	0.938	0.955	0.973	0.982	0.991	0.999	0.999	0.999	0.999	0.999	
smMALA	$\mathbb{R}^d$	0.58	0.593	0.599	0.632	0.576	0.694	0.733	0.805	0.866	0.934	0.495	0.588	0.678	0.768	0.858	0.211	0.307	0.397	0.484	0.571	0.658	0.745	0.832	0.911	0.981	0.993	0.999	0.999	0.999	0.999	0.999	0.999	0.999	0.999		
smMALA <sub>0</sub>	$\mathbb{R}^d$	0.58	0.401	0.43	0.532	0.183	0.388	0.346	0.333	0.222	0.26	0.653	0.801	0.588	0.281	0.348	0.59	0.645	0.619	0.683	0.711	0.757	0.857	0.945	0.984	0.993	0.999	0.999	0.999	0.999	0.999	0.999	0.999	0.999	0.999		
MAPLA	$\mathbb{R}^d$	0.138	0.148	0.137	0.179	0.253	0.319	0.683	0.719	0.758	0.811	0.635	0.685	0.648	0.544	0.514	0.472	0.521	0.583	0.621	0.676	0.725	0.787	0.849	0.919	0.981	0.993	0.999	0.999	0.999	0.999	0.999	0.999	0.999	0.999		
MAPLA <sub>0</sub>	$\mathbb{R}^d$	0.103	0.15	0.177	0.142	0.201	0.319	0.405	0.471	0.501	0.624	0.544	0.585	0.624	0.472	0.521	0.583	0.621	0.676	0.725	0.787	0.849	0.919	0.981	0.993	0.999	0.999	0.999	0.999	0.999	0.999	0.999	0.999				
LHR	$\mathbb{R}^d$	0.207	0.147	0.157	0.171	0.241	0.319	0.522	0.591	0.658	0.722	0.532	0.577	0.614	0.417	0.473	0.538	0.591	0.658	0.722	0.789	0.857	0.919	0.981	0.993	0.999	0.999	0.999	0.999	0.999	0.999	0.999	0.999				
stLR	$\mathbb{R}^d$	0.241	0.208	0.226	0.191	0.313	0.388	0.532	0.455	0.474	0.519	0.491	0.534	0.534	0.385	0.417	0.473	0.538	0.591	0.658	0.722	0.789	0.857	0.919	0.981	0.993	0.999	0.999	0.999	0.999	0.999	0.999	0.999	0.999			
smLR	$\mathbb{R}^d$	0.557	0.52	0.596	0.515	0.621	0.644	0.735	0.777	0.817	0.857	0.534	0.586	0.626	0.462	0.521	0.575	0.631	0.688	0.722	0.789	0.857	0.919	0.981	0.993	0.999	0.999	0.999	0.999	0.999	0.999	0.999	0.999				
smLR <sub>0</sub>	$\mathbb{R}^d$	0.535	0.578	0.578	0.644	0.521	0.621	0.624	0.656	0.695	0.736	0.534	0.586	0.626	0.462	0.521	0.575	0.631	0.688	0.722	0.789	0.857	0.919	0.981	0.993	0.999	0.999	0.999	0.999	0.999	0.999	0.999	0.999				
smLR <sub>0.5</sub>	$\mathbb{R}^d$	0.535	0.578	0.578	0.644	0.521	0.621	0.624	0.656	0.695	0.736	0.534	0.586	0.626	0.462	0.521	0.575	0.631	0.688	0.722	0.789	0.857	0.919	0.981	0.993	0.999	0.999	0.999	0.999	0.999	0.999	0.999	0.999				
smLR <sub>0.9</sub>	$\mathbb{R}^d$	0.535	0.578	0.578	0.644	0.521	0.621	0.624	0.656	0.695	0.736	0.534	0.586	0.626	0.462	0.521	0.575	0.631	0.688	0.722	0.789	0.857	0.919	0.981	0.993	0.999	0.999	0.999	0.999	0.999	0.999	0.999	0.999				
smLR <sub>0.95</sub>	$\mathbb{R}^d$	0.535	0.578	0.578	0.644	0.521	0.621	0.624	0.656	0.695	0.736	0.534	0.586	0.626	0.462	0.521	0.575	0.631	0.688	0.722	0.789	0.857	0.919	0.981	0.993	0.999	0.999	0.999	0.999	0.999	0.999	0.999	0.999				
smLR <sub>0.99</sub>	$\mathbb{R}^d$	0.535	0.578	0.578	0.644	0.521	0.621	0.624	0.656	0.695	0.736	0.534	0.586	0.626	0.462	0.521	0.575	0.631	0.688	0.722	0.789	0.857	0.919	0.981	0.993	0.999	0.999	0.999	0.999	0.999	0.999	0.999	0.999				
smLR <sub>0.995</sub>	$\mathbb{R}^d$	0.535	0.578	0.578	0.644	0.521	0.621	0.624	0.656	0.695	0.736	0.534	0.586	0.626	0.462	0.521	0.575	0.631	0.688	0.722	0.789	0.857	0.919	0.981	0.993	0.999	0.999	0.999	0.999	0.999	0.999	0.999	0.999				
smLR <sub>0.999</sub>	$\mathbb{R}^d$	0.535	0.578	0.578	0.644	0.521	0.621	0.624	0.656	0.695	0.736	0.534	0.586	0.626	0.462	0.521	0.575	0.631	0.688	0.722	0.789	0.857	0.919	0.981	0.993	0.999	0.999	0.999	0.999	0.999	0.999	0.999	0.999				
smLR <sub>0.9995</sub>	$\mathbb{R}^d$	0.535	0.578	0.578	0.644	0.521	0.621	0.624	0.656	0.695	0.736	0.534	0.586	0.626	0.462	0.521	0.575	0.631	0.688	0.722	0.789	0.857	0.919	0.981	0.993	0.999	0.999	0.999	0.999	0.999	0.999	0.999	0.999				
smLR <sub>0.9999</sub>	$\mathbb{R}^d$	0.535	0.578	0.578	0.644	0.521	0.621	0.624	0.656	0.695	0.736	0.534	0.586	0.626	0.462	0.521	0.575	0.631	0.688	0.722	0.789	0.857	0.919	0.981	0.993	0.999	0.999	0.999	0.999	0.999	0.999	0.999	0.999				
smLR <sub>0.99995</sub>	$\mathbb{R}^d$	0.535	0.578	0.578	0.644	0.521	0.621	0.624	0.656	0.695	0.736	0.534	0.586	0.626	0.462	0.521	0.575	0.631	0.688	0.722	0.789	0.857	0.919	0.981	0.993	0.999	0.999	0.999	0.999	0.999	0.999	0.999	0.999				
smLR <sub>0.99999</sub>	$\mathbb{R}^d$	0.535	0.578	0.578	0.644	0.521	0.621	0.624	0.656	0.695	0.736	0.534	0.586	0.626	0.462	0.521	0.575	0.631	0.688	0.722	0.789	0.857	0.919	0.981	0.993	0.999	0.999	0.999	0.999	0.999	0.999	0.999	0.999				
smLR <sub>0.999995</sub>	$\mathbb{R}^d$	0.535	0.578	0.578	0.644	0.521	0.621	0.624	0.656	0.695	0.736	0.534	0.586	0.626	0.462	0.521	0.575	0.631	0.688	0.722	0.789	0.857	0.919	0.981	0.993	0.999	0.999	0.999	0.999	0.999	0.999	0.999	0.999				
smLR <sub>0.999999</sub>	$\mathbb{R}^d$	0.535	0.578	0.578	0.644	0.521	0.621	0.624	0.656	0.695	0.736	0.534	0.586	0.626	0.462	0.521	0.575	0.631	0.688	0.722	0.789	0.857	0.919	0.981	0.993	0.999	0.999	0.999	0.999	0.999	0.999	0.999	0.999				
smLR <sub>0.9999995</sub>	$\mathbb{R}^d$	0.535	0.578	0.578	0.644	0.521	0.621	0.624	0.656	0.695	0.736	0.534	0.586	0.626	0.462	0.521	0.575	0.631	0.688	0.722	0.789	0.857	0.919	0.981	0.993	0.999	0.999	0.999	0.999	0.999	0.999	0.999	0.999				
smLR <sub>0.9999999</sub>	$\mathbb{R}^d$	0.535	0.578	0.578	0.644	0.521	0.621	0.624	0.656	0.695	0.736	0.534	0.586	0.626	0.462	0.521	0.575	0.631	0.688	0.722	0.789	0.857	0.919	0.981	0.993	0.999	0.999	0.999	0.999	0.999	0.999	0.999	0.999				
smLR <sub>0.99999995</sub>	$\mathbb{R}^d$	0.535	0.578	0.578	0.644	0.521	0.621	0.624	0.656	0.695	0.736	0.534	0.586	0.626	0.462	0.521	0.575	0.631	0.688	0.722	0.789	0.857	0.919	0.981	0.993	0.999	0.999	0.999	0.999	0.999	0.999	0.999	0.999				
smLR <sub>0.99999999</sub>	$\mathbb{R}^d$	0.535	0.578	0.578	0.644	0.521	0.621	0.624	0.656	0.695	0.736	0.534	0.586	0.626	0.462	0.521	0.575	0.631	0.688	0.722	0.789	0.857	0.919	0.981	0.993	0.999	0.999	0.999	0.999	0.999	0.999	0.999	0.999				
smLR <sub>0.999999995</sub>	$\mathbb{R}^d$	0.535	0.578	0.578	0.644	0.521	0.621	0.624	0.656	0.695	0.736	0.534	0.586	0.626	0.462	0.521	0.575	0.631	0.688	0.722	0.789	0.857	0.919	0.981	0.993	0.999	0.999	0.999	0.999	0.999	0.999	0.999	0.999				
smLR <sub>0.999999999</sub>	$\mathbb{R}^d$	0.535	0.578	0.578	0.644	0.521	0.621	0.624	0.656	0.695	0.736	0.534	0.586	0.626	0.462	0.521	0.575	0.631	0.688	0.722	0.789	0.857	0.919	0.981	0.993	0.999	0.999	0.999	0.999	0.999	0.999	0.999	0.999				
smLR <sub>0.9999999995</sub>	$\mathbb{R}^d$	0.535	0.578	0.578	0.644	0.521	0.621	0.624	0.656	0.695	0.736	0.534	0.586	0.626	0.462	0.521	0.575	0.631	0.688	0.722	0.789	0.857	0.919	0.981	0.993	0.999	0.999	0.999	0.999	0.999	0.999	0.999	0.999				
smLR <sub>0.9999999999</sub>	$\mathbb{R}^d$	0.535	0.578	0.578	0.644	0.521	0.621																														

Table 7: Average relative performance based on minEFSs of the tested samplers across dimensions as presented as solid lines in Fig. 10.

Table 8: Average relative performance based on minESS/s of the tested samplers across polytope angles as presented as solid lines in Fig. 10.

Sampler	Target	Gauss ( $\mu = 0$ )		Cigr ( $\mu = 0$ )		Gauss ( $\mu = 0.5$ )		Cigr ( $\mu = 0.5$ )		Bowie		Funnel	
		9°	19°	9°	19°	9°	19°	9°	19°	9°	19°	9°	19°
RWMH	0.01	0.057	0.102	0.213	0.031	0.106	0.413	0.353	0.033	0.348	0.455	0.066	0.343
MALA	0.01	0.102	0.168	0.312	0.035	0.156	0.547	0.647	0.036	0.334	0.686	0.016	0.398
smMALA	0.141	0.162	0.248	0.473	0.002	0.077	0.224	0.262	0.043	0.327	0.495	0.064	0.507
smMALA <sub>0.5</sub>	0.009	0.137	0.247	0.577	0.044	0.152	0.532	0.657	0.041	0.328	0.521	0.063	0.576
Dikin	0.309	0.165	0.310	0.123	0.078	0.954	0.573	0.522	0.066	0.446	0.577	0.168	0.899
MAPLA	0.234	0.124	0.081	0.126	0.647	0.581	0.337	0.344	0.298	0.252	0.287	0.165	0.091
HR	0.048	0.113	0.243	0.299	0.15	0.34	0.871	0.786	0.175	0.495	0.831	0.090	0.33
LHR	0.035	0.161	0.433	0.41	0.128	0.363	0.855	0.798	0.141	0.503	0.856	0.043	0.447
smHR	0.084	0.172	0.359	0.625	0.039	0.069	0.075	0.668	0.173	0.302	0.788	0.076	0.453
smLHR	0.204	0.493	0.874	0.574	0.005	0.13	0.519	0.338	0.077	0.192	0.512	0.858	0.743
smNLHR	0.204	0.493	0.874	0.574	0.005	0.13	0.519	0.338	0.077	0.192	0.512	0.858	0.743

Table 9: Average relative performance based on minESS/s of the tested samplers across densities' scale parameter as presented as solid lines in Fig. 10.

Sampler	Target	Gauss ( $\mu = 0$ )				Disc ( $\mu = 0$ )				Cigar ( $\mu = 0$ )				Gauss ( $\mu = 0.5$ )				
		$\sigma$	$10^{-2}$	$10^{-1.5}$	$10^{-1}$	$10^0$	$10^{-2}$	$10^{-1.5}$	$10^{-1}$	$10^0$	$10^{-1.5}$	$10^{-1}$	$10^0$	$10^{-2}$	$10^{-1.5}$	$10^{-1}$	$10^0$	
RWMLA	0.034	0.035	0.033	0.097	0.212	0.49	<b>0.547</b>	0.452	0.473	0.49	0.464	0.471	0.425	0.555	0.453	0.437	0.447	0.486
MLALA	0.071	0.055	0.051	0.146	0.286	0.584	<b>0.546</b>	0.625	0.555	0.52	0.532	0.558	0.618	0.588	0.472	0.43	0.489	0.536
smMLA	<b>0.848</b>	<b>0.117</b>	<b>0.733</b>	<b>0.701</b>	<b>0.676</b>	<b>0.558</b>	0.524	0.126	0.077	0.057	0.048	0.06	0.106	0.129	0.399	0.417	0.403	0.459
smMLA <sub>1</sub>	0.497	0.584	0.171	0.555	0.568	0.354	0.366	0.383	0.409	0.391	0.403	0.474	0.366	0.431	0.414	0.433	0.485	0.537
DirIn	0.141	0.188	0.167	0.173	0.201	0.259	<b>0.674</b>	0.678	0.709	0.71	<b>0.721</b>	<b>0.667</b>	<b>0.695</b>	<b>0.641</b>	<b>0.624</b>	<b>0.588</b>	0.569	0.535
MAPLA	0.082	0.104	0.112	0.114	0.158	0.224	0.225	0.355	0.348	0.363	0.402	0.472	0.498	0.332	0.353	0.339	0.403	0.466
HR	0.012	0.017	0.018	0.036	0.101	0.249	0.183	0.216	0.219	0.229	0.237	0.283	0.163	0.176	0.194	0.223	0.316	0.411
LIR	0.03	0.029	0.034	0.069	0.157	0.272	0.295	0.18	0.14	0.208	0.185	0.246	0.223	0.173	0.216	0.212	0.246	0.301
smHR	0.18	0.238	0.26	0.265	0.405	0.496	0.056	0.053	0.041	0.058	0.081	0.166	0.196	0.215	0.312	0.301	0.305	0.388
smHR <sub>1</sub>	0.153	0.183	0.218	0.233	0.398	0.511	0.524	0.175	0.183	0.027	0.192	0.245	0.267	0.284	0.167	0.158	0.222	0.324
smHR <sub>2</sub>	0.299	0.338	0.404	0.324	0.391	0.376	0.339	0.326	0.326	0.03	0.055	0.061	0.071	0.181	0.251	0.247	0.263	0.315
smHR <sub>3</sub>	0.205	0.19	0.283	0.21	0.244	0.305	0.287	0.168	0.172	0.204	0.202	0.226	0.223	0.189	0.151	0.204	0.248	0.359

Table 10: Average relative performance based on minESS/s of the tested samplers across densities’ scale parameter as presented as solid lines in Fig 10

Table 11: Average L1 error of the tested samplers across dimensions as presented as solid lines in Fig. 11.

Sampler	Target	Gauss ( $\mu = 0$ )	Disc ( $\mu = 0$ )	Cigar ( $\mu = 0$ )	Gauss ( $\mu = 0.5$ )	Disc ( $\mu = 0.5$ )	Cigar ( $\mu = 0.5$ )	Gauss ( $\mu = 1$ )	Disc ( $\mu = 1$ )	Cigar ( $\mu = 1$ )	Gauss ( $\mu = 1.5$ )	Disc ( $\mu = 1.5$ )	Cigar ( $\mu = 1.5$ )	Gauss ( $\mu = 2$ )	Disc ( $\mu = 2$ )	Cigar ( $\mu = 2$ )	Gauss ( $\mu = 3$ )	Disc ( $\mu = 3$ )	Cigar ( $\mu = 3$ )	Gauss ( $\mu = 4$ )	Disc ( $\mu = 4$ )	Cigar ( $\mu = 4$ )	Gauss ( $\mu = 8$ )	Disc ( $\mu = 8$ )	Cigar ( $\mu = 8$ )	Gauss ( $\mu = 16$ )	Disc ( $\mu = 16$ )	Cigar ( $\mu = 16$ )	Gauss ( $\mu = 32$ )	Disc ( $\mu = 32$ )	Cigar ( $\mu = 32$ )	Gauss ( $\mu = 64$ )	Disc ( $\mu = 64$ )	Cigar ( $\mu = 64$ )	Gauss ( $\mu = 128$ )	Disc ( $\mu = 128$ )	Cigar ( $\mu = 128$ )	Gauss ( $\mu = 256$ )	Disc ( $\mu = 256$ )	Cigar ( $\mu = 256$ )	Gauss ( $\mu = 512$ )	Disc ( $\mu = 512$ )	Cigar ( $\mu = 512$ )	Gauss ( $\mu = 1024$ )	Disc ( $\mu = 1024$ )	Cigar ( $\mu = 1024$ )	Gauss ( $\mu = 2048$ )	Disc ( $\mu = 2048$ )	Cigar ( $\mu = 2048$ )	Gauss ( $\mu = 4096$ )	Disc ( $\mu = 4096$ )	Cigar ( $\mu = 4096$ )	Gauss ( $\mu = 8192$ )	Disc ( $\mu = 8192$ )	Cigar ( $\mu = 8192$ )	Gauss ( $\mu = 16384$ )	Disc ( $\mu = 16384$ )	Cigar ( $\mu = 16384$ )	Gauss ( $\mu = 32768$ )	Disc ( $\mu = 32768$ )	Cigar ( $\mu = 32768$ )	Gauss ( $\mu = 65536$ )	Disc ( $\mu = 65536$ )	Cigar ( $\mu = 65536$ )	Gauss ( $\mu = 131072$ )	Disc ( $\mu = 131072$ )	Cigar ( $\mu = 131072$ )	Gauss ( $\mu = 262144$ )	Disc ( $\mu = 262144$ )	Cigar ( $\mu = 262144$ )	Gauss ( $\mu = 524288$ )	Disc ( $\mu = 524288$ )	Cigar ( $\mu = 524288$ )	Gauss ( $\mu = 1048576$ )	Disc ( $\mu = 1048576$ )	Cigar ( $\mu = 1048576$ )	Gauss ( $\mu = 2097152$ )	Disc ( $\mu = 2097152$ )	Cigar ( $\mu = 2097152$ )	Gauss ( $\mu = 4194304$ )	Disc ( $\mu = 4194304$ )	Cigar ( $\mu = 4194304$ )	Gauss ( $\mu = 8388608$ )	Disc ( $\mu = 8388608$ )	Cigar ( $\mu = 8388608$ )	Gauss ( $\mu = 16777216$ )	Disc ( $\mu = 16777216$ )	Cigar ( $\mu = 16777216$ )	Gauss ( $\mu = 33554432$ )	Disc ( $\mu = 33554432$ )	Cigar ( $\mu = 33554432$ )	Gauss ( $\mu = 67108864$ )	Disc ( $\mu = 67108864$ )	Cigar ( $\mu = 67108864$ )	Gauss ( $\mu = 134217728$ )	Disc ( $\mu = 134217728$ )	Cigar ( $\mu = 134217728$ )	Gauss ( $\mu = 268435456$ )	Disc ( $\mu = 268435456$ )	Cigar ( $\mu = 268435456$ )	Gauss ( $\mu = 536870912$ )	Disc ( $\mu = 536870912$ )	Cigar ( $\mu = 536870912$ )	Gauss ( $\mu = 107374184$ )	Disc ( $\mu = 107374184$ )	Cigar ( $\mu = 107374184$ )	Gauss ( $\mu = 214748368$ )	Disc ( $\mu = 214748368$ )	Cigar ( $\mu = 214748368$ )	Gauss ( $\mu = 429496736$ )	Disc ( $\mu = 429496736$ )	Cigar ( $\mu = 429496736$ )	Gauss ( $\mu = 858993472$ )	Disc ( $\mu = 858993472$ )	Cigar ( $\mu = 858993472$ )	Gauss ( $\mu = 1717986944$ )	Disc ( $\mu = 1717986944$ )	Cigar ( $\mu = 1717986944$ )	Gauss ( $\mu = 3435973888$ )	Disc ( $\mu = 3435973888$ )	Cigar ( $\mu = 3435973888$ )	Gauss ( $\mu = 6871947776$ )	Disc ( $\mu = 6871947776$ )	Cigar ( $\mu = 6871947776$ )	Gauss ( $\mu = 1374389552$ )	Disc ( $\mu = 1374389552$ )	Cigar ( $\mu = 1374389552$ )	Gauss ( $\mu = 2748778104$ )	Disc ( $\mu = 2748778104$ )	Cigar ( $\mu = 2748778104$ )	Gauss ( $\mu = 5497556208$ )	Disc ( $\mu = 5497556208$ )	Cigar ( $\mu = 5497556208$ )	Gauss ( $\mu = 1099511216$ )	Disc ( $\mu = 1099511216$ )	Cigar ( $\mu = 1099511216$ )	Gauss ( $\mu = 2199022432$ )	Disc ( $\mu = 2199022432$ )	Cigar ( $\mu = 2199022432$ )	Gauss ( $\mu = 4398044864$ )	Disc ( $\mu = 4398044864$ )	Cigar ( $\mu = 4398044864$ )	Gauss ( $\mu = 8796089728$ )	Disc ( $\mu = 8796089728$ )	Cigar ( $\mu = 8796089728$ )	Gauss ( $\mu = 1759217944$ )	Disc ( $\mu = 1759217944$ )	Cigar ( $\mu = 1759217944$ )	Gauss ( $\mu = 3518435888$ )	Disc ( $\mu = 3518435888$ )	Cigar ( $\mu = 3518435888$ )	Gauss ( $\mu = 7036871776$ )	Disc ( $\mu = 7036871776$ )	Cigar ( $\mu = 7036871776$ )	Gauss ( $\mu = 1407374352$ )	Disc ( $\mu = 1407374352$ )	Cigar ( $\mu = 1407374352$ )	Gauss ( $\mu = 2814748704$ )	Disc ( $\mu = 2814748704$ )	Cigar ( $\mu = 2814748704$ )	Gauss ( $\mu = 5629497408$ )	Disc ( $\mu = 5629497408$ )	Cigar ( $\mu = 5629497408$ )	Gauss ( $\mu = 1125899488$ )	Disc ( $\mu = 1125899488$ )	Cigar ( $\mu = 1125899488$ )	Gauss ( $\mu = 2251798976$ )	Disc ( $\mu = 2251798976$ )	Cigar ( $\mu = 2251798976$ )	Gauss ( $\mu = 4503597952$ )	Disc ( $\mu = 4503597952$ )	Cigar ( $\mu = 4503597952$ )	Gauss ( $\mu = 9007197904$ )	Disc ( $\mu = 9007197904$ )	Cigar ( $\mu = 9007197904$ )	Gauss ( $\mu = 1801439584$ )	Disc ( $\mu = 1801439584$ )	Cigar ( $\mu = 1801439584$ )	Gauss ( $\mu = 3602879168$ )	Disc ( $\mu = 3602879168$ )	Cigar ( $\mu = 3602879168$ )	Gauss ( $\mu = 7205758336$ )	Disc ( $\mu = 7205758336$ )	Cigar ( $\mu = 7205758336$ )	Gauss ( $\mu = 1441151672$ )	Disc ( $\mu = 1441151672$ )	Cigar ( $\mu = 1441151672$ )	Gauss ( $\mu = 2882303344$ )	Disc ( $\mu = 2882303344$ )	Cigar ( $\mu = 2882303344$ )	Gauss ( $\mu = 5764606688$ )	Disc ( $\mu = 5764606688$ )	Cigar ( $\mu = 5764606688$ )	Gauss ( $\mu = 1152921376$ )	Disc ( $\mu = 1152921376$ )	Cigar ( $\mu = 1152921376$ )	Gauss ( $\mu = 2305842752$ )	Disc ( $\mu = 2305842752$ )	Cigar ( $\mu = 2305842752$ )	Gauss ( $\mu = 4611685504$ )	Disc ( $\mu = 4611685504$ )	Cigar ( $\mu = 4611685504$ )	Gauss ( $\mu = 9223371008$ )	Disc ( $\mu = 9223371008$ )	Cigar ( $\mu = 9223371008$ )	Gauss ( $\mu = 1844674208$ )	Disc ( $\mu = 1844674208$ )	Cigar ( $\mu = 1844674208$ )	Gauss ( $\mu = 3689348416$ )	Disc ( $\mu = 3689348416$ )	Cigar ( $\mu = 3689348416$ )	Gauss ( $\mu = 7378696832$ )	Disc ( $\mu = 7378696832$ )	Cigar ( $\mu = 7378696832$ )	Gauss ( $\mu = 14757393664$ )	Disc ( $\mu = 14757393664$ )	Cigar ( $\mu = 14757393664$ )	Gauss ( $\mu = 29514787328$ )	Disc ( $\mu = 29514787328$ )	Cigar ( $\mu = 29514787328$ )	Gauss ( $\mu = 59029574656$ )	Disc ( $\mu = 59029574656$ )	Cigar ( $\mu = 59029574656$ )	Gauss ( $\mu = 11805914912$ )	Disc ( $\mu = 11805914912$ )	Cigar ( $\mu = 11805914912$ )	Gauss ( $\mu = 23611829824$ )	Disc ( $\mu = 23611829824$ )	Cigar ( $\mu = 23611829824$ )	Gauss ( $\mu = 47223659648$ )	Disc ( $\mu = 47223659648$ )	Cigar ( $\mu = 47223659648$ )	Gauss ( $\mu = 9444731920$ )	Disc ( $\mu = 9444731920$ )	Cigar ( $\mu = 9444731920$ )	Gauss ( $\mu = 18889463840$ )	Disc ( $\mu = 18889463840$ )	Cigar ( $\mu = 18889463840$ )	Gauss ( $\mu = 37778927680$ )	Disc ( $\mu = 37778927680$ )	Cigar ( $\mu = 37778927680$ )	Gauss ( $\mu = 75557855360$ )	Disc ( $\mu = 75557855360$ )	Cigar ( $\mu = 75557855360$ )	Gauss ( $\mu = 15111571040$ )	Disc ( $\mu = 15111571040$ )	Cigar ( $\mu = 15111571040$ )	Gauss ( $\mu = 30223142080$ )	Disc ( $\mu = 30223142080$ )	Cigar ( $\mu = 30223142080$ )	Gauss ( $\mu = 60446284160$ )	Disc ( $\mu = 60446284160$ )	Cigar ( $\mu = 60446284160$ )	Gauss ( $\mu = 120892568320$ )	Disc ( $\mu = 120892568320$ )	Cigar ( $\mu = 120892568320$ )	Gauss ( $\mu = 241785136640$ )	Disc ( $\mu = 241785136640$ )	Cigar ( $\mu = 241785136640$ )	Gauss ( $\mu = 483570273280$ )	Disc ( $\mu = 483570273280$ )	Cigar ( $\mu = 483570273280$ )	Gauss ( $\mu = 967140546560$ )	Disc ( $\mu = 967140546560$ )	Cigar ( $\mu = 967140546560$ )	Gauss ( $\mu = 193428109120$ )	Disc ( $\mu = 193428109120$ )	Cigar ( $\mu = 193428109120$ )	Gauss ( $\mu = 386856218240$ )	Disc ( $\mu = 386856218240$ )	Cigar ( $\mu = 386856218240$ )	Gauss ( $\mu = 773712436480$ )	Disc ( $\mu = 773712436480$ )	Cigar ( $\mu = 773712436480$ )	Gauss ( $\mu = 154742487280$ )	Disc ( $\mu = 154742487280$ )	Cigar ( $\mu = 154742487280$ )	Gauss ( $\mu = 309484974560$ )	Disc ( $\mu = 309484974560$ )	Cigar ( $\mu = 309484974560$ )	Gauss ( $\mu = 618969949120$ )	Disc ( $\mu = 618969949120$ )	Cigar ( $\mu = 618969949120$ )	Gauss ( $\mu = 123793989840$ )	Disc ( $\mu = 123793989840$ )	Cigar ( $\mu = 123793989840$ )	Gauss ( $\mu = 247587979680$ )	Disc ( $\mu = 247587979680$ )	Cigar ( $\mu = 247587979680$ )	Gauss ( $\mu = 495175959360$ )	Disc ( $\mu = 495175959360$ )	Cigar ( $\mu = 495175959360$ )	Gauss ( $\mu = 990351918720$ )	Disc ( $\mu = 990351918720$ )	Cigar ( $\mu = 990351918720$ )	Gauss ( $\mu = 1980703837440$ )	Disc ( $\mu = 1980703837440$ )	Cigar ( $\mu = 1980703837440$ )	Gauss ( $\mu = 3961407674880$ )	Disc ( $\mu = 3961407674880$ )	Cigar ( $\mu = 3961407674880$ )	Gauss ( $\mu = 7922815349600$ )	Disc ( $\mu = 7922815349600$ )	Cigar ( $\mu = 7922815349600$ )	Gauss ( $\mu = 1584563079200$ )	Disc ( $\mu = 1584563079200$ )	Cigar ( $\mu = 1584563079200$ )	Gauss ( $\mu = 3169128158400$ )	Disc ( $\mu = 3169128158400$ )	Cigar ( $\mu = 3169128158400$ )	Gauss ( $\mu = 6338256316800$ )	Disc ( $\mu = 6338256316800$ )	Cigar ( $\mu = 6338256316800$ )	Gauss ( $\mu = 1267651233600$ )	Disc ( $\mu = 1267651233600$ )	Cigar ( $\mu = 1267651233600$ )	Gauss ( $\mu = 2535302467200$ )	Disc ( $\mu = 2535302467200$ )	Cigar ( $\mu = 2535302467200$ )	Gauss ( $\mu = 5070604934400$ )	Disc ( $\mu = 5070604934400$ )	Cigar ( $\mu = 5070604934400$ )	Gauss ( $\mu = 10141209868800$ )	Disc ( $\mu = 10141209868800$ )	Cigar ( $\mu = 10141209868800$ )	Gauss ( $\mu = 20282419737600$ )	Disc ( $\mu = 20282419737600$ )	Cigar ( $\mu = 20282419737600$ )	Gauss ( $\mu = 40564839475200$ )	Disc ( $\mu = 40564839475200$ )	Cigar ( $\mu = 40564839475200$ )	Gauss ( $\mu = 8112967890400$ )	Disc ( $\mu = 8112967890400$ )	Cigar ( $\mu = 8112967890400$ )	Gauss ( $\mu = 16225935708800$ )	Disc ( $\mu = 16225935708800$ )	Cigar ( $\mu = 16225935708800$ )	Gauss ( $\mu = 32451871417600$ )	Disc ( $\mu = 32451871417600$ )	Cigar ( $\mu = 32451871417600$ )	Gauss ( $\mu = 64903742835200$ )	Disc ( $\mu = 64903742835200$ )	Cigar ( $\mu = 64903742835200$ )	Gauss ( $\mu = 12980748566400$ )	Disc ( $\mu = 12980748566400$ )	Cigar ( $\mu = 12980748566400$ )	Gauss ( $\mu = 25961497132800$ )	Disc ( $\mu = 25961497132800$ )	Cigar ( $\mu = 25961497132800$ )	Gauss ( $\mu = 51922994265600$ )	Disc ( $\mu = 51922994265600$ )	Cigar ( $\mu = 51922994265600$ )	Gauss ( $\mu = 10384598851200$ )	Disc ( $\mu = 10384598851200$ )	Cigar ( $\mu = 10384598851200$ )	Gauss ( $\mu = 20769197702400$ )	Disc ( $\mu = 20769197702400$ )	Cigar ( $\mu = 20769197702400$ )	Gauss ( $\mu = 41538395404800$ )	Disc ( $\mu = 41538395404800$ )	Cigar ( $\mu = 41538395404800$ )	Gauss ( $\mu = 83076790809600$ )	Disc ( $\mu = 83076790809600$ )	Cigar ( $\mu = 83076790809600$ )	Gauss ( $\mu = 16615358161600$ )	Disc ( $\mu = 16615358161600$ )	Cigar ( $\mu = 16615358161600$ )	Gauss ( $\mu = 33230716323200$ )	Disc ( $\mu = 33230716323200$ )	Cigar ( $\mu = 33230716323200$ )	Gauss ( $\mu = 66461424646400$ )	Disc ( $\mu = 66461424646400$ )	Cigar ( $\mu = 66461424646400$ )	Gauss ( $\mu = 13292289289600$ )	Disc ( $\mu = 13292289289600$ )	Cigar ( $\mu = 13292289289600$ )	Gauss ( $\mu = 26584578579200$ )	Disc ( $\mu = 26584578579200$ )	Cigar ( $\mu = 26584578579200$ )	Gauss ( $\mu = 53169157584000$ )	Disc ( $\mu = 53169157584000$ )	Cigar ( $\mu = 53169157584000$ )	Gauss ( $\mu = 106338311152000$ )	Disc ( $\mu = 106338311152000$ )	Cigar ( $\mu = 106338311152000$ )	Gauss ( $\mu = 212676622304000$ )	Disc ( $\mu = 212676622304000$ )	Cigar ( $\mu = 212676622304000$ )	Gauss ( $\mu = 425353244608000$ )	Disc ( $\mu = 425353244608000$ )	Cigar ( $\mu = 425353244608000$ )	Gauss ( $\mu = 850706489216000$ )	Disc ( $\mu = 850706489216000$ )	Cigar ( $\mu = 850706489216000$ )	Gauss ( $\mu = 170141289432000$ )	Disc ( $\mu = 170141289432000$ )	Cigar ( $\mu = 170141289432000$ )	Gauss ( $\mu = 340282578864000$ )	Disc ( $\mu = 340282578864000$ )	Cigar ( $\mu = 340282578864000$ )	Gauss ( $\mu = 680565157728000$ )	Disc ( $\mu = 680565157728000$ )	Cigar ( $\mu = 680565157728000$ )	Gauss ( $\mu = 1361130354560000$ )	Disc ( $\mu = 1361130354560000$ )	Cigar ( $\mu = 1361130354560000$ )	Gauss ( $\mu = 2722260709120000$ )	Disc ( $\mu = 2722260709120000$ )	Cigar ( $\mu = 2722260709120000$ )	Gauss ( $\mu = 5444521418240000$ )	Disc ( $\mu = 5444521418240000$ )	Cigar ( $\mu = 5444521418240000$ )	Gauss ( $\mu = 10889042836800000$ )	Disc ( $\mu = 10889042836800000$ )	Cigar ( $\mu = 10889042836800000$ )	Gauss ( $\mu = 21778085673600000$ )	Disc ( $\mu = 21778085673600000$ )	Cigar ( $\mu = 21778085673600000$ )	Gauss ( $\mu = 43556171347200000$ )	Disc ( $\mu = 43556171347200000$ )	Cigar ( $\mu = 43556171347200000$ )	Gauss ( $\mu = 87112342694400000$ )	Disc ( $\mu = 87112342694400000$ )	Cigar ( $\mu = 87112342694400000$ )	Gauss ( $\mu = 174224685388800000$ )	Disc ( $\mu = 174224685388800000$ )	Cigar ( $\mu = 174224685388800000$ )	Gauss ( $\mu = 348449371776000000$ )	Disc ( $\mu = 348449371776000000$ )	Cigar ( $\mu = 348449371776000000$ )	Gauss ( $\mu = 696898743552000000$ )	Disc ( $\mu = 696898743552000000$ )	Cigar ( $\mu = 696898743552000000$ )	Gauss ( $\mu = 1393797487040000000$ )	Disc ( $\mu = 1393797487040000000$ )	Cigar ( $\mu = 1393797487040000000$ )	Gauss ( $\mu = 2787594974080000000$ )	Disc ( $\mu = 2787594974080000000$ )	Cigar ( $\mu = 2787594974080000000$ )	Gauss ( $\mu = 5575188948160000000$ )	Disc ( $\mu = 55751$